Imaging proto-oceanic crust off the Brazilian Continental Margin

F Klingelhoefer, Michel Evain, A Afilhado, C Rigoti, A Loureiro, D Alves, Angélique Leprêtre, M Moulin, P Schnurle, M Benabdellouahed, et al.

Geophysical Journal International

Geophys. J. Int. (2015) **200,** 471–488 doi: 10.1093/gji/ggu387

GJI Marine geosciences and applied geophysics

Imaging proto-oceanic crust off the Brazilian Continental Margin

F. Klingelhoefer,[1] M. Evain,[1] A. Afilhado,[1,2] C. Rigoti,[3] A. Loureiro,[2] D. Alves,[2] A. Leprêtre,[1] M. Moulin,[1] P. Schnurle,[1] M. Benabdellouahed,[1] A. Baltzer,[4] M. Rabineau,[5] A. Feld,[6] A. Viana[3] and D. Aslanian[1]

[1] *Ifremer, Department of Marine Geosciences, Z.I. de la Pointe du Diable, F-*29280 *Plouzané, France. E-mail: frauke.klingelhoefer@ifremer.fr*
[2] *IDL – Instituto Dom Luis, Lisboa, Faculdade das Ciências da Universidade de Lisboa,* 1749-016 *Lisboa, Portugal*
[3] *Petrobras, Petrobras Research Center, Rio de Janeiro, Brazil*
[4] *Géolittomer, LETG UMR* 6554*-CNRS, Institut de Géographie et d'Aménagement Régional de l'Université de Nantes, BP* 81227*, F-*44312 *Nantes Cedex* 3*, France*
[5] *Domaines Océaniques, UMR*6538*, Institut Universitaire Européen de la mer,* 1*-place Copernic, F-*29280 *Plouzané, France*
[6] *Genavir, DEC/QAE, Centre de Brest de l'Ifremer, Z.I. de la Pointe du Diable, F-*29280 *Plouzané, France*

Accepted 2014 October 3. Received 2014 October 3; in original form 2014 June 12

SUMMARY

During the Sanba (*San*tos *ba*sin seismic transect) experiment in 2010–2011, a 380-km-long combined wide-angle and reflection seismic profile has been acquired using 30 ocean-bottom seismometers, a 4.5 km seismic streamer and a 8900 in.^{3} airgun array. The Sanba 3 profile crosses the southern flank of the Sao Paulo Plateau, the Sao Paulo Ridge and the easternmost Santos Basin in an east–west direction. Its eastern end is located on undisturbed oceanic crust. Tomographic and forward modelling of the wide-angle seismic data reveals that the sedimentary thickness is variable with only 1–2 km on top of the ridge and thickening to 4–5 km in the basin. Crustal thickness at the ridge is about 18 km and the relative layer thickness and velocity gradients indicate a continental origin of this ridge. The eastern Santos Basin is underlain by crust of only 5 km thickness, characterized by high seismic velocities between 6.20 km s^{-1} in the upper crust and 7.40 km s^{-1} in the lower crust. Three hypotheses for the nature of the crust in this region are tested here: (i) thinned continental crust, (ii) serpentinized upper mantle material, (iii) thin oceanic crust. As seismic velocity gradients seem to rule out a continental origin of this region, and clear Moho reflections argue against serpentinized upper mantle, we propose that the crust underlying the easternmost Santos Basin is of oceanic origin. Deviations from normal oceanic crustal velocities in the lower crust (6.70–7.00 km s^{-1}) can be explained by accretion at slow spreading rates leading to the inclusion of serpentinite into the lower crust at the onset of organized seafloor spreading.

Key words: Controlled source seismology; Seismic tomography; Mid-ocean ridge processes; Continental margins: divergent; Continental tectonics: extensional; Crustal structure; South America.

1 INTRODUCTION

While accretion of oceanic crust is well studied at present-day spreading centres, many open questions remain regarding the formation of early oceanic crust following rupture of a continent. The boundary between continental and oceanic crust can hardly be expected to be abrupt. During the initial phase of opening and at very slow spreading rates and accordingly low mantle temperatures, most of the material available may originate from the upper mantle. Little melt can be extracted from the mantle to form igneous oceanic crust, leading to a proto-oceanic crust including basaltic flow on top of a layer of serpentinized upper mantle material. When the spreading rate increases, more vigorous mantle upwelling can occur providing more melt and leading to the formation of thin igneous oceanic crust at first and normal oceanic crust in a later stage. Recent studies of the Ocean Drilling Project (ODP) drilling samples from the continent–ocean transition zone of the Newfoundland and Iberia margin suggest that the transition from rifting to magmatic seafloor spreading is not well defined but transitional over a period of ∼15 Myr (Jagoutz *et al.* 2007). The authors propose that during juvenile, ultraslow spreading, phases with MORB-type magmatic activity alternated with tectonic spreading phases.

In this study, we present wide-angle and reflection seismic data of a profile located 650 km off the Brasilian coast on top of the São Paulo Ridge and crossing the neighbouring easternmost Santos Basin. Although several marine investigations have been conducted in the easternmost Santos Basin its origin is still debated (e.g. Leyden *et al.* 1971; Meisling *et al.* 2001; Zalan *et al.* 2011; Fig. 1).

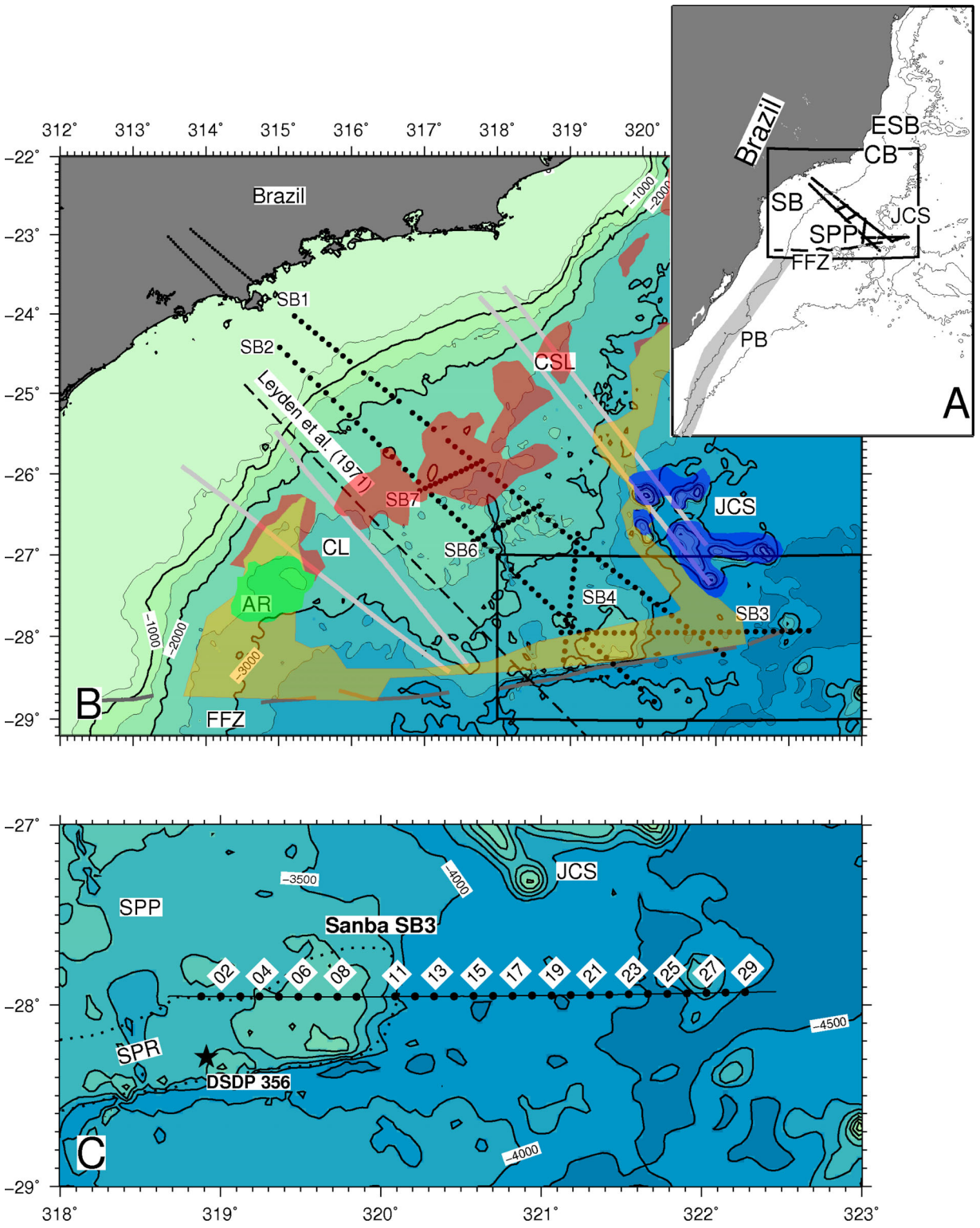

Figure 1. (a) Regional bathymetry map. SB, Santon Basin; FFZ, Florianopolis fracture zone; PB, Pelotas Basin; CB, Campos Basin; ESB, Espitio Santo Basin; JCS, Jean Charcot Seamounts; AR, Abimael Ridge; CSL, Cruzeiro do Sul Lineament; CL, Capricornio Lineament; SPP, Sao-Paulo Plateau; SPR, Sao Paulo Ridge. Frame shows extension of zoom (b) and grey polygone marks the extension of seaward dipping reflectors in the Pelotas Basin (Blaich *et al.* 2011; Hinz *et al.* 1999). (b) Bathymetry of the Santos Basin and location of the wide-angle seismic profiles of the SANBA experiment. Black circles mark seafloor instrument positions, dashed line the deep seismic profile BB′ of Leyden *et al.* (1971), yellow polygones position of the serpentinized upper mantle as proposed by Zalan *et al.* (2011), orange polygones position of the failed spreading centre as proposed by Meisling *et al.* (2001), green polygone Abimael Ridge and blue polygone position of the Jean Charcot Seamounts. Outlined box marks the position of the zoom (c) Bathymetry of the research area along profile Sanba 3. Black circles mark OBS positions and black line the shot positions. Position of DSDP drill hole 356 is marked by a star. Grey area marks extend of the Sao Paule Ridge from Kumar & Gamboa (1979).

Zalan *et al.* (2011) proposed, on the base of deep sounding reflection seismic profiles and gravity modelling, the presence of exhumed mantle in the easternmost Santos Basin. Moulin *et al.* (2010) propose based on plate-kinematic reconstructions an oceanic origin for the crust underlying this basin.

The origin of the neighbouring São Paulo Ridge is equally debated today. While Zalan *et al.* (2011) proposed, the presence of exhumed mantle overlain by volcanic layers on the São Paulo Ridge, Kumar *et al.* (2012) using the same set of data and following Henry *et al.* (2010), Scotchman *et al.* (2010) and Alvey *et al.* (2011), proposed it to be of continental nature. This last hypothesis is in good agreement with the kinematic reconstructions proposed by Moulin *et al.* 2012, which include a continental microblock at the São Paulo Ridge.

The Sanba 3 profile, part of the Sanba project, which aims at constraining the crustal structure and the geodynamic settings of the SSPS, is a 380-km-long wide-angle and reflection seismic profile acquired about 600–700 km off the Brazilian coast in a strictly east–west direction (Fig. 1). The western part is located on a well-known basement high, the Sao Paulo Plateau and the middle and eastern part in the adjacent basin.

2 GEOLOGIC SETTING AND PREVIOUS WORK

The Santos Basin–Sao Paulo Plateau System (SSPS) is located at the boundary between the Central Segment and the Austral Segment of the South Atlantic Ocean, and can be interpreted as a kinematic 'buffer' zone (Moulin *et al.* 2010; Moulin *et al.* 2012). While the southern Austral Segment opened between anomalies M13 and M4 (Rabinowitz & LaBrecque 1979; Austin & Uchupi 1982; Curie 1984; Moulin *et al.* 2010), 139.5 and 130 Ma, respectively (Gradstein *et al.* 2004), oceanic spreading in the Central Segment started more than 18 Ma later, at the end of evaporite deposition (Upper Aptian–Lower Albian: 112 Ma; Rabinowitz & LaBrecque 1979; Curie 1984; Torsvik *et al.* 2009; Moulin *et al.* 2010).

The evolution of the The Santos Basin–São Paulo Plateau system (SSPS) was proposed to be related to a ridge jump or a ridge propagator advancing northwards (Kumar & Gamboa 1979; Mohriak 2001). However, the formation of the SSPS and its narrow conjugate Namibe margin can be explained by the buffer role of the Santos subplate, with a southward directed propagating ridge originating from the Central Segment and producing the strike-slip direction given by the movement of the microblocks, extending along the Namibe margin explain (Moulin *et al.* 2012).

The Santos Basin–SSPS is situated immediately north of the Florianópolis (or Rio Grande) fracture zone (FFZ), which separates a domain of magma-rich continental margin with large and continuous seaward dipping reflectors (SDRs) to the south, from a moderately volcanic margin characterized by Aptian salt deposits to the north (Stica *et al.* 2014). Industrial ultradeep seismic lines from the Pelotas basin show abundant SDRs and rifts completely filled by volcanic rocks (Stica *et al.* 2014).

During one of the first deep seismic studies along in the Santos Basin a combined reflection and expanding-spread-profiles (ESP) study was conducted (Fig. 1a; Leyden *et al.* 1971). Combining 14 ESPs along a profile in the Santos Basin, the continent–ocean transition could be roughly imaged, as ESP data allow for a very good vertical resolution but only a poor lateral resolution. Sedimentary thickness varied between 1 and 3 km along the profile. Moho depth near the coast was about 15 km decreasing to only about 10 km in the basin. Crust to the SE of the FFZ was interpreted to be of oceanic origin. Mantle velocities were constrained to be around 8 km s^{-1}, except at the SE end of the profile where the highest velocities were 7.4 km s^{-1} in only 10 km depth (Leyden *et al.* 1971). In this region the crust was modelled to be only about 4–5 km thick and interpreted to be of oceanic origin.

An along-strike segmentation of the Campos and Santos continental margin by Early Cretaceous transfer zones was inferred from sparse public domain seismic profiles and gravity data (Meisling *et al.* 2001). The transfer zones were identified by high-angle faults in seismic sections and interpolated between profiles using the gravity data. The existence of pre-rift volcanic highs led the authors to propose the existence of a failed spreading centre, Abimael Ridge, in the SSPS about 300 km off the Brazilian coast leading to true oceanic crust 400 km offshore, about 150 km closer than previous studies (Leyden *et al.* 1971; Fig. 1).

The interpretation of 12 000 km of deep sounding reflection seismic data, coupled with gravimetric and magnetometric modelling, provided a first 3-D view of the deep structure of the Santos, Campos and Espirito Santo Basin (Zalan *et al.* 2011). Through most of the study region the brittle upper crust gave only poor reflections, with the exception of some distinctive subhorizontal reflections cutting the crust diagonally, and interpreted to be intracrustal simple shear zones (Zalan *et al.* 2011). A highly reflective lower crustal layer was observed throughout the study area (Fig. 1). The authors interpreted a large area of proposed exhumed and serpentinized upper mantle material. Serpentinization was deduced to occur down to several kilometers depth by gravity modelling (yellow band in Fig. 1a; C. Rigoti, personal communication).

The Sao Paulo Plateau is located about 650 km offshore the Brazilian coast in a water depth of approximately 2500 m. The Sao Paulo Ridge marks the southern boundary of the plateau and is bounded to the south by the FFZ (Fig. 1). The early refraction work by Leyden *et al.* (1971) indicated that the eastern edge of the Plateau coincides roughly with the eastern limit of a salt diapir zone extending from the coast throughout the basin. In order to investigate the plate tectonic setting in which salt was deposited, DSDP bore hole 356 was drilled on the Sao Paulo Ridge (Perch-Nielsen & Supko 1977). Unfortunately basement was not reached during drilling operations due to time constraints. However, and in good agreement with the existing wide-angle seismic data, the existence of continental crust at the Sao Paulo Plateau has been proposed from reflection seismic data and gravity modelling (Chang *et al.* 1992; Blaich *et al.* 2011). In contrast with these interpretations, Kumar & Gamboa (1979) deduce that the Sao Paulo Plateau is a marginal plateau underlain by oceanic crust from correlation of sedimentary structures. From reflection seismic profiles and the fact that basalt fragments were drilled at the position of DSDP bore hole 356 on the Sao Paulo Ridge the authors conclude that the ridge is composed of mafic igneous rocks.

3 OBJECTIVES OF THE CRUISE

The main objectives for the acquisition of the Sanba 3 profile were to constrain the nature of the crust of the easternmost part of the Sao Paulo Plateau, in order to better understand the original opening scenario of this part of the Atlantic Ocean and to identify the origin of the crust underlying the adjacent basin. Testing of the hypothesis, that the Santos Basin in this region is underlain by exhumed upper mantle material (Zalan *et al.* 2011) can provide information about the style of rifting, for example symmetric pure shear type

rifting (McKenzie 1978), simple shear type (Wernicke 1985) or non-conservative rifting style (Aslanian *et al.* 2009; Aslanian & Moulin 2012).

4 SEISMIC DATA

The Sanba marine research cruise was conducted on R/V L'Atalante during in 2010 December and 2011 January. The combined reflection and wide-angle seismic profile Sanba 3 is located in water depths between 2500 and 4500 m and 29 4-channel (1 hydrophone and 3 geophone) ocean–bottom seismometers were deployed along the profile at an interval of about 12 km. One instrument was lost, but all others recorded successfully on all channels. A seismic source consisting of a tuned array of 18 air-guns with a combined volume of 8900 in.^{3} was used to fire 2370 low frequency shots along the profile. The shots were additionally recorded by a 360-channel 4.5-km-long digital seismic streamer.

The processing sequence of the reflection seismic data was composed of geometry (including streamer feathering), CMP binning at 12.5 m interval and sorting, bandpass filter (2–16–64–96 Hz), re-sampling from 2 to 4 ms (Fig. 2). After velocity analysis, true amplitude recovery was applied, normal moveout, multiple attenuation, time-variant bandpass filter (from 2–16–48–64 at sea bottom to 2–16–32–48 Hz 3 s below), inside and outside mute, stack and post-stack time-variant bandpass filter and Kirchhoff time migration. Two passes of semblance velocity analysis (every 500 then 250 cdp) were performed. Multiple attenuation was achieved with an FK-filter applied to supergathers of 4 cdps (half fold at 25 m trace interval).

Pre-processing of the OBS data included calculation of the clock-drift corrections to adjust the clock in each instrument to the GPS base time. Instrument locations were corrected for drift from the deployment position during their descent to the seafloor using the direct water wave arrival. The drift of all instruments did not exceed 200 m. All instruments recovered gave useful data on all four channels (Fig. 3). Data quality along the profile was generally very good with clear arrivals to offsets over 100 km between the ship and the seafloor instrument (Fig. 2). Picking of the onset of first and secondary arrivals was performed without filtering where possible (mostly between offsets of 0 and 40 km). Further processing of the data to facilitate picking at further offsets included deconvolution, application of a 5–15 Hz Butterworth filter and trace normalization.

4.1 Tomographic inversion

The tomographic inversion code FAST (Zelt & Barton 1998) was further used to construct a first velocity model (Fig. 4). This model also served as an initial guideline to the forward modelling, described hereafter. This non-linear tomographic approach consists in a regularized inversion in which user specified parameters weight the final solution in terms of traveltime misfit and model roughness. The method is linearized in that a starting model and iterative convergence scheme are employed. Nonlinearity is accounted for by calculating new ray paths at each iteration. The method generates smooth models which do not resolve sharp boundaries, but it can represent sharp velocity boundaries as steep gradients. The most important structural features are thus resolved in an objective manner. Additional information from secondary arrivals and gravity modelling were not incorporated into the inversion in order to keep the approach objective. In order to perform this tomographic inversion of the first arrivals, 17 413 traveltimes have been picked along the complete profile. 47.2 per cent of the picks were done on offsets larger than 35 km, which is a first estimate for crossover distances of upper mantle arrivals on oceanic crust. The tomographic model used a grid of 410 km × 30 km with a 0.5 km grid cell size (Fig. 4). Keeping the initial model as simple as possible avoids incorporation of artefacts resulting from the initial model into the final results. For this model it consisted of two layers, one layer from the sea bottom up to 12 km depth with velocities ranging from 3.0 to 7.5 km s^{-1} and a second layer from 12 to 40 km depth with velocities ranging from 7.5 to 8.2 km s^{-1}. The water velocity was kept constant at 1.5 km s^{-1}. For the final model run, five different lambda values

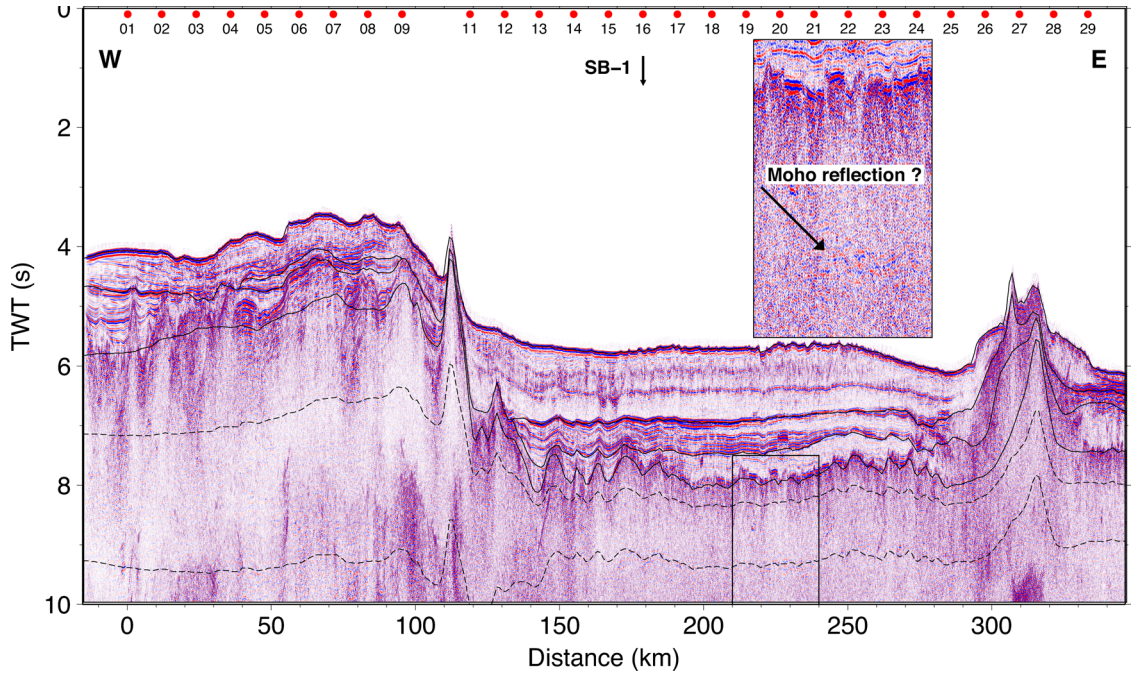

Figure 2. Multichannel seismic section of profile Sanba 3. The final velocity model from forward modelling converted to TWTT is overlain.

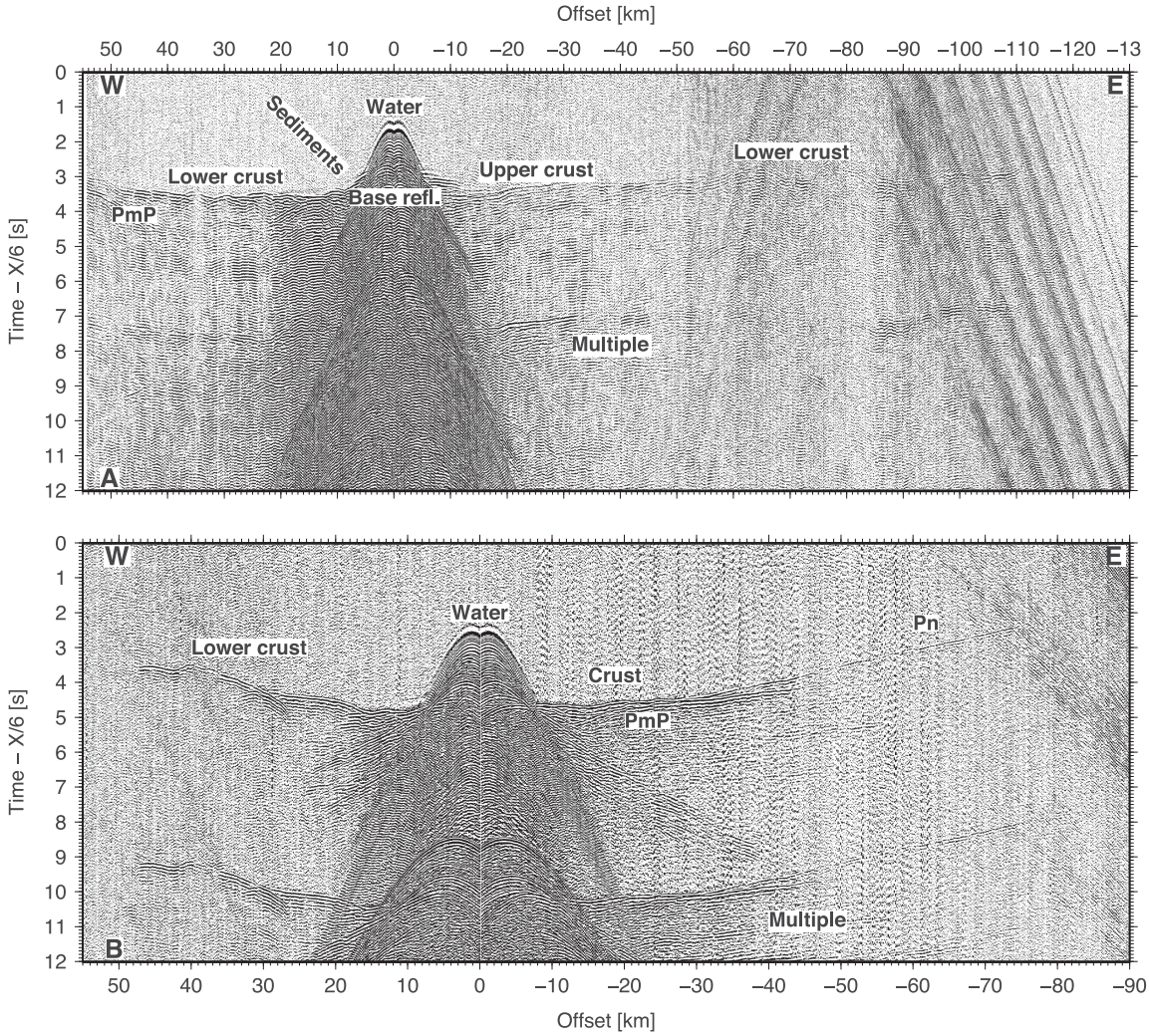

Figure 3. Data sections of OBS 04 and 15 (a) bandpass filtered data from OBS 04, geophone channel. The data are displayed with gain proportional to source–receiver offset and are reduced at a velocity of 6 km s^{-1}. Main phases are labelled. (b) Bandpass filtered (3–5 Hz, 24–36 Hz) data from OBS 15, geophone channel. The data are displayed as in (a).

were tested in 10 non-linear iterative steps, where lambda is the trade-off parameter that controls the weighting of data misfit versus the constraint equations. After 10 iterations the model misfit does not decrease significantly, and small unrealistic velocity anomalies begin to appear in the velocity model.

4.2 Forward modelling

The data were modelled using a 2-D iterative damped least-squares traveltime inversion from the RAYINVR software (Zelt & Smith 1992; Zelt 1999). Modelling was performed using a layer-stripping approach, proceeding from the top of the structure towards the bottom. Upper layers were adjusted to improve the fit of lower layers where not directly constrained by arrivals from within the layer. Arrival times of the main sedimentary layers and basement were picked from the reflection seismic data (Fig. 2). These were converted to depth using the OBS data. The depth and velocities of the crustal layers and the upper mantle were modelled from the OBS data only.

The final velocity model shows the depth geometry of all sedimentary layers and the basement (Fig. 5). Sedimentary velocities vary between 2.0 and 2.3 km s^{-1} in the first, between 2.4 and 3.2 km s^{-1} in the second and between 3.0 and 3.6 km s^{-1} in the third layer. A high-velocity layer was detected between sedimentary layer 1 and 3 at model distances between 40 and 100 km. This layer is characterized by velocities between 4.5 and 4.7 km s^{-1}.

Throughout the profile two crustal layers were modelled. Their combined thickness ranges from 18 km at the Sao Paulo Ridge to 5 km in the easternmost Santos Basin. Two prominent basement highs were modelled at 100 and 300 km model distance. Velocities of these layers range between 5.40 and 7.00 km s^{-1}. Moho depth varies between 18 km underneath the eastern part of the profile and 12 km in the basin itself. Upper-mantle velocities were 8.00–8.20 km s^{-1} throughout the model.

4.3 Error calculation

4.3.1 Tomographic model

The fit between predicted arrival times and traveltime picks provides information about the quality of the model, and can be described by the root-mean-square error (RMSE; Fig. 6). The final tomographic model is characterized by a RMSE of 170 ms, mainly due to relatively large traveltime errors for rays returning from the deeper

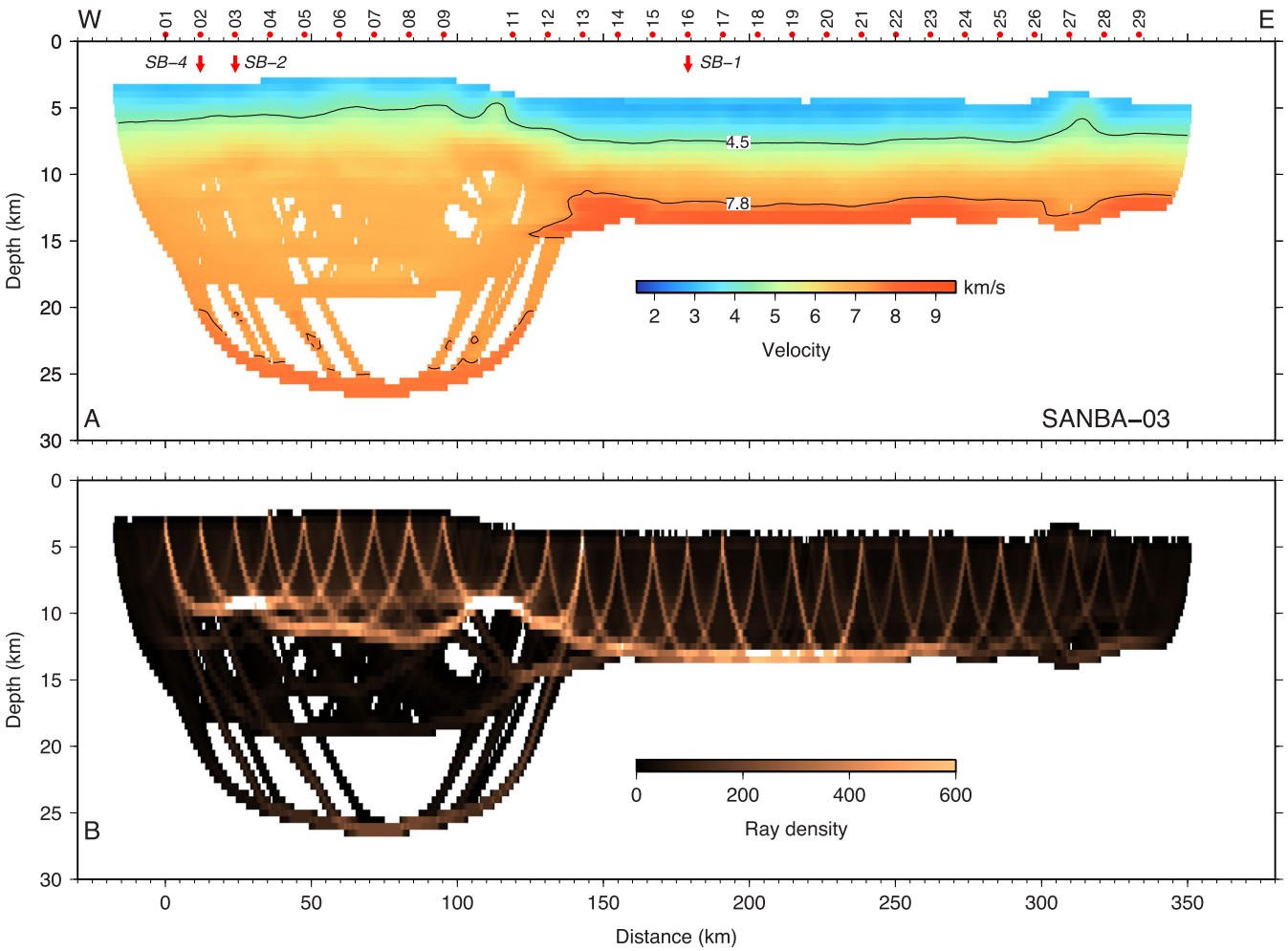

Figure 4. (a) Result of the tomographic inversion of first arrivals on a 0.5 km × 0.5 km grid. The 4.5 and the 7.8 km s^{-1} iso-velocity contours are trace to give a rough estimate of basement and Moho depth along the profile. OBS locations are indicated by red circles. The 4.5 and 7.8 km s^{-1} isocontours representing the basement and the Moho are contoured. (b) Ray density of the final tomographic model (0.5 km × 0.5 km).

regions of the western part of the model (Fig. 4b). This is confirmed by the ray coverage, which is generally very good (Fig. 4b), except for depths larger than 20 km in the western part of the model. Thus, the tomographic code cannot successfully reproduce the lower crust in this region, probably due to relatively sparse arrivals and the fact that reflected arrivals from the Moho are not taken into account.

Checkerboard tests using synthetic data were performed in order to constrain the resolution of the model in different depths using the given experiment geometry. Synthetic models consisting of sinusoidal anomalies were superimposed onto the final velocity model of Fig. 4(a). The maximum amplitude of the anomalies in the synthetic models is +5 and −5 per cent of the background velocity. Synthetic arrival times with the same source–receiver geometry as in the data set used for the final results, have been generated for these models. Synthetic noise was added to the traveltimes for each of the checkerboard tests. The result of the inversions after one iteration starting from the reference model of Fig. 4 and using the synthetic data set and the differences between the synthetic and inverted models are displayed in Fig. 7. The largest anomalies tested (40 km × 15 km) can be resolved very well to depths up to 20 km and but are smeared in depths from 20 to 30 km. Smaller sized anomalies (20 km × 10 km) are resolved equally well up to 20 km, but are not reproduced at depths greater than 20 km. Anomalies of the size of 10 km × 5 km are resolved well in the upper layers up to 10 km depth and the smallest sized anomalies tested (5 km × 4 km) are resolved mainly in the western part of the model for depth up to 8–10 km. The checkerboard tests confirm that regions deeper than 20 km between 0 and 40 km model distance are relatively less well constrained as compared to other parts of the model.

4.3.2 Forward model

The fit between the model and the traveltime picks is given by the RMSE. The number of picks, the picking error, the values for the χ^2 parameter and the rms misfit are given in Table 1 for each phase. The ray coverage of the forward model is slightly higher than for the tomographic model, due to the secondary phases and reflections which have additionally been introduced in the model (Figs 8b and 5b). The RMSE of the forward model is lower (119 ms) than for the tomographic model.

Perturbation of the velocity and the depth of a single horizon allows the assessment of the velocity and depth uncertainties. Fig. 9 shows the variation of the RMSE for all relevant phases for a depth perturbation of the Moho and a velocity perturbation of the lower crustal layer. The depth of the bottom of the layer was varied between −0.2 and +0.2 km and the velocities between −0.5 and +0.5

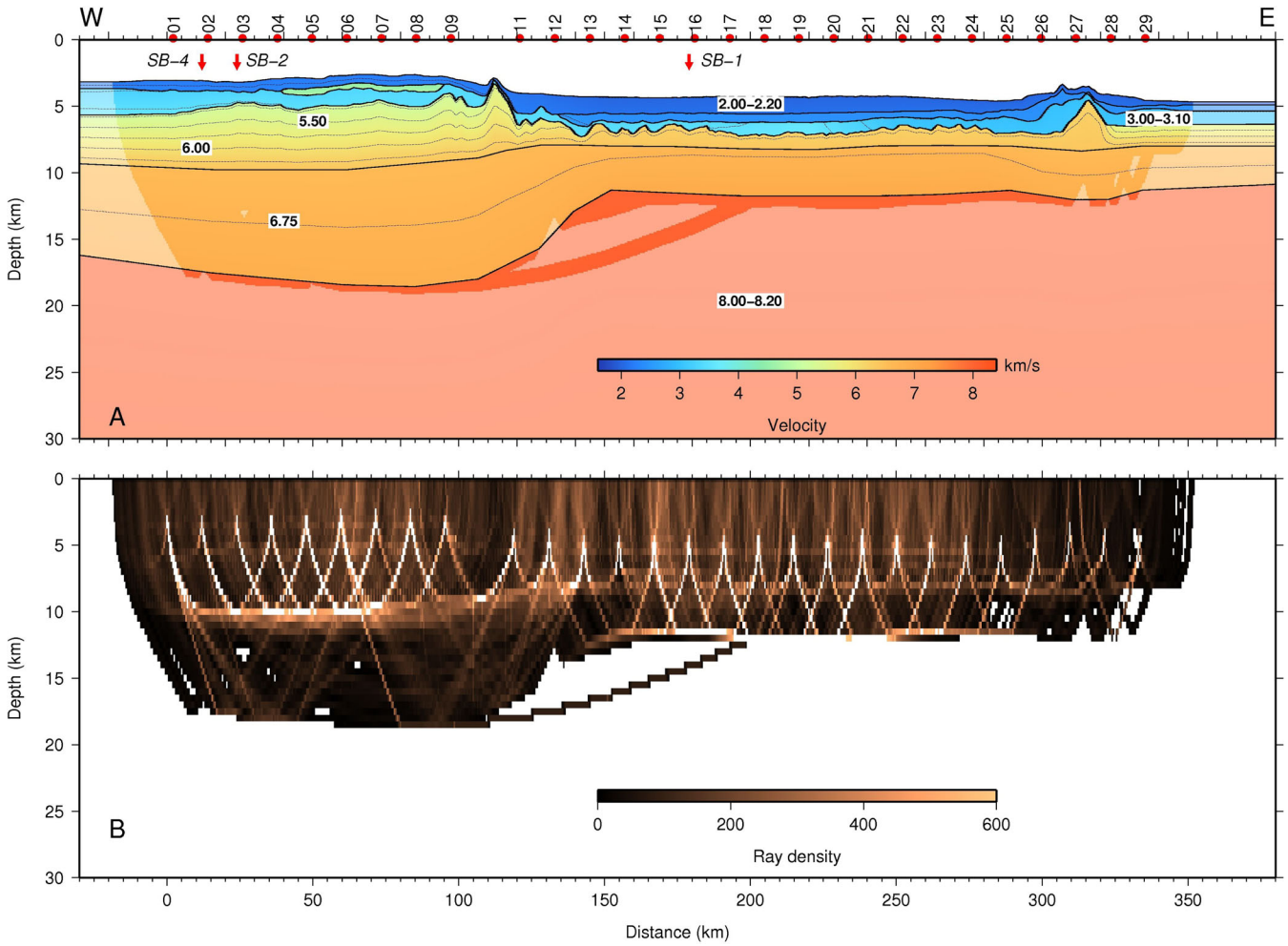

Figure 5. (a) Final velocity model of profile Sanba 3. Velocities are contoured at an 0.25 km s^{-1} interval and black lines mark layer boundaries from the modelling. Shaded areas are unconstrained by seismic rays. Red circles mark obs positions and arrows cross point with profiles SB-1 and SB-4. (b) Ray density on a 0.5 km × 0.5 km grid).

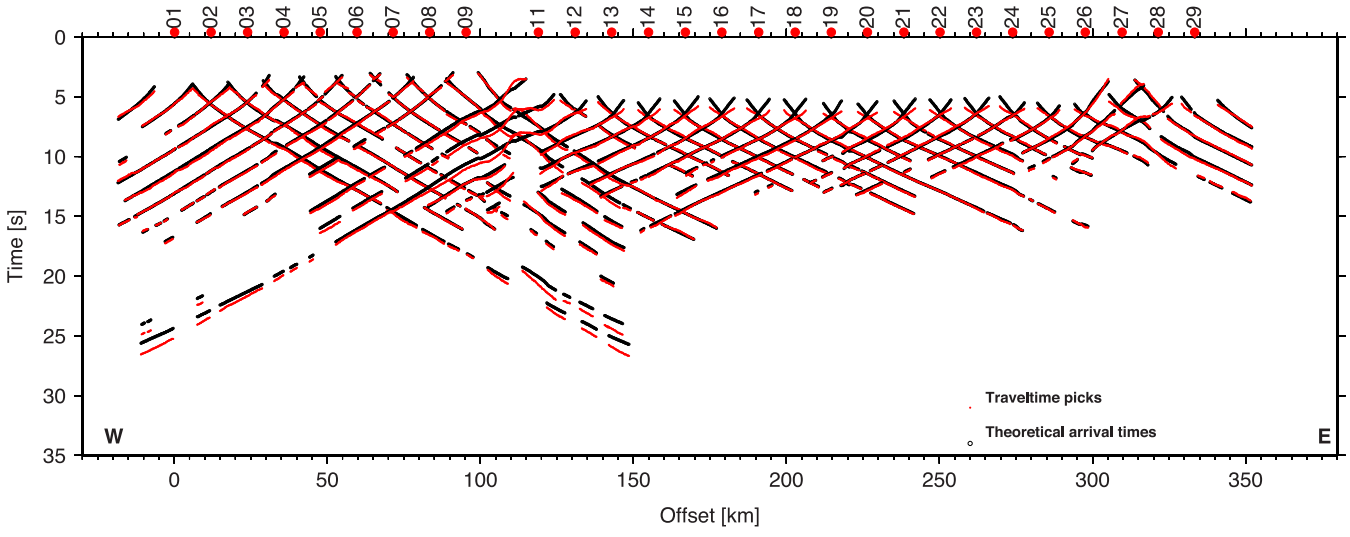

Figure 6. First arrival traveltime picks and theoretical arrivals predicted by the tomographic approach.

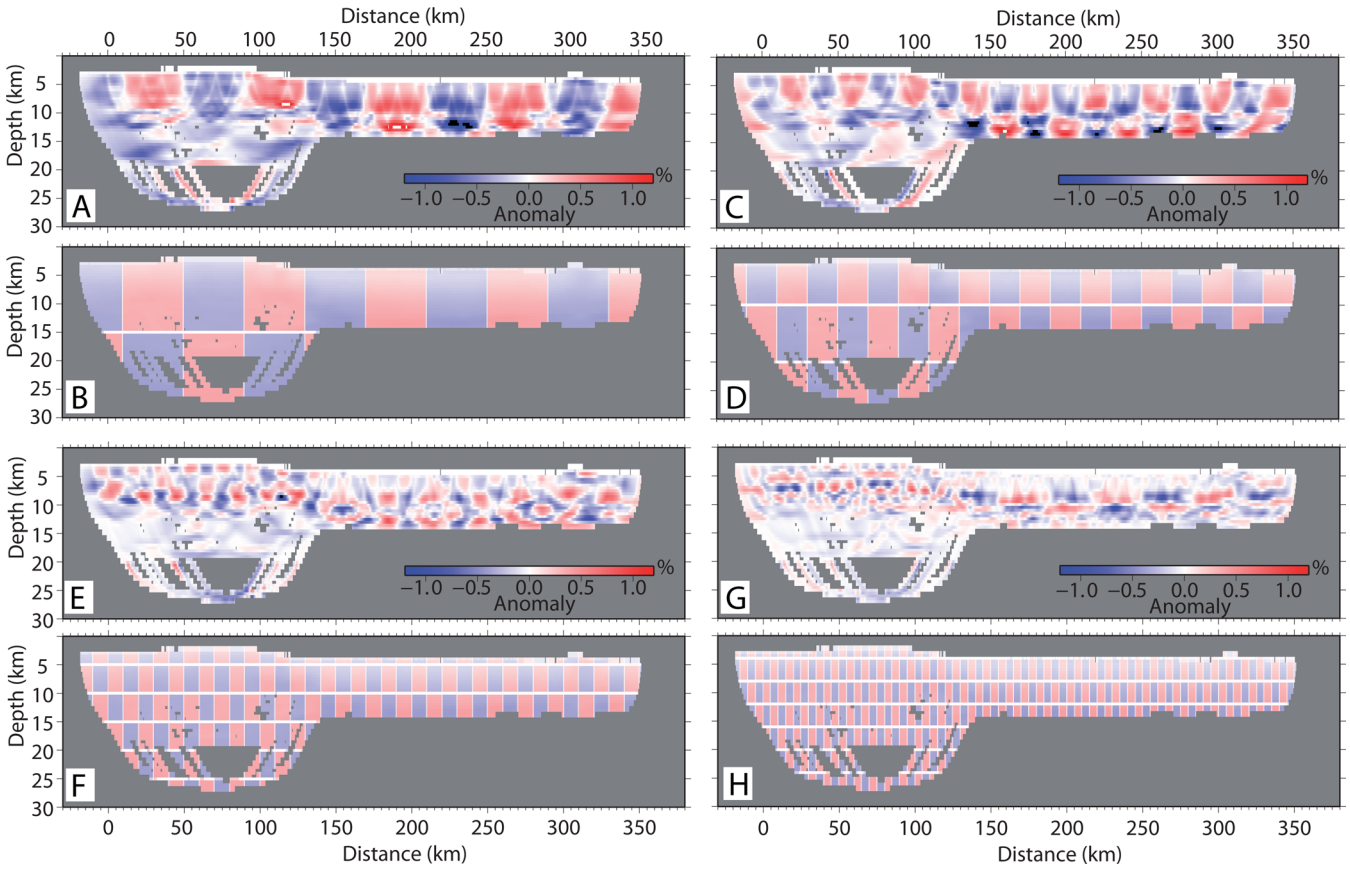

Figure 7. Results of the checkerboard test. (a) Test result including anomalies of the size 40 km × 15 km. (b) Synthetic anomalies of the size 40 km × 15 km. (c) Test result including anomalies of the size 20 km × 10 km. (d) synthetic anomalies of the size 20 km × 10 km. (e) Test result including anomalies of the size 10 km × 5 km. (f) synthetic anomalies of the size 10 km × 5 km. (g) Test result including anomalies of the size 5 km × 4 km. (h) synthetic anomalies of the size 5 km × 4 km.

Table 1. Phase names, number of picks and RMSE for all phases.

Name of the phase	Number of picks	RMSE (ms)
Water	2113	0.022
Sediments 1	1716	0.099
Sediments 2	401	0.106
Sediments 3	795	0.124
Basement	2136	0.152
Basement reflection	713	0.095
Lower crust	6430	0.124
PmP	1423	0.119
Pn	3514	0.098
Sill	119	0.095

km s^{-1}. Analysis of the results show that all combinations reaching RMSEs below 120 ms are located in the range of velocities used for the final model.

Additional information about the quality of the velocity model can be gained from the resolution parameter (Fig. 10; Zelt & Smith 1992). Resolution is a measure of the number of rays passing through a region of the model constrained by a particular velocity node. As the method of Zelt & Smith (1992) uses a sparsely parametrized inversion, the resolution depends on the node spacing, whereas they are unrelated in a regularized inversion, such as the FAST tomography. If a layer can be modelled with one single velocity gradient, the resolution parameter will be high even in areas which have lower ray coverage, since the area is related to only one velocity node. The advantage of this representation is that it allows an assessment of whether all lateral velocity changes are required by the data. Nodes with values greater than 0.5 are considered well resolved (Fig. 10). The uppermost and lowermost sedimentary layers and the crustal layers are well resolved. In the easternmost segment between 80 and 110 km model distance, the velocities of the low-velocity layer underneath of what it is interpreted as basalt are not constrained by turning rays. Thus, this layer shows a low resolution. Also the second sedimentary layer is not well resolved, as its layer thickness is not high enough to allow rays to turn in this layer. The geometry of these two regions is mainly constrained by the reflection seismic data. Upper-mantle velocities are only well constrained, especially as the upper-mantle velocity is constant throughout the profile. Hence no structures unconstrained by the data have been included in the model (Zelt 1999).

In order to estimate the velocity and depth uncertainty of the final velocity model a perturbation analysis was performed. The depths of key interfaces were varied and an F test was applied to determine if a significant change between models could be detected. The 95 per cent confidence limit gives an estimate of the depth uncertainty of the interface (Fig. 9). The Moho is constrained to +0.4/−0.5 km and the mid-crustal reflector to +0.3/−0.3 km.

In order to constrain the velocity gradients of the different layers, synthetic seismograms were calculated and compared to the data sections. The finite difference modelling code from the Seismic Unix package (Stockwell 1999; Cohen & Stockwell 2003) was

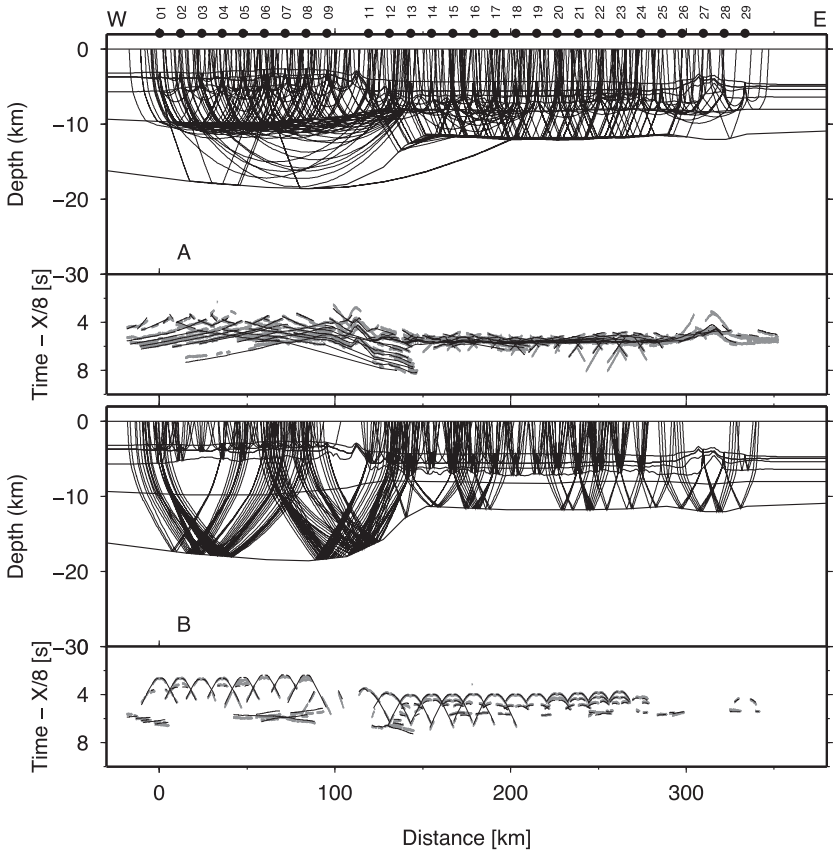

Figure 8. (a) Upper panel: ray coverage due to all arrivals from turning rays. Lower panel: traveltime picks and predicted arrivals times for all arrivals from turning rays. (b) Upper panel: ray coverage due to all arrivals from reflected rays. Lower panel: traveltime picks and predicted arrivals times for all arrivals from reflected rays.

used to calculate synthetic seismograms of a record length of 30 s at a 100 m spacing (Figs 11 and 12). The program uses the explicit second order differencing method for modelling the acoustic wave equation. The input velocity model was calculated from sampling the forward velocity model at a lateral 50 m interval and 10 m interval in depth. In order to avoid grid dispersion, the peak frequency of the Ricker wavelet source signal is calculated to be equal to the lowest velocity of the medium divided by the grid points per wavelength multiplied by 10. In this case the source wavelet is centred at 8 Hz, similar to the signal from the airgun array used during the cruise. The boundary conditions were set to be absorbing at the sides and bottom of the model and free at the surface. The observed and calculated amplitudes generally show a good fit, with relatively strong amplitude PmP arrivals underneath the Sao Paulo Ridge and weaker amplitude PmP arrivals in the basin. Pn arrivals are characterized by weak amplitudes throughout the model, as velocity gradients in the upper mantle are low.

4.4 Gravity modelling

Gravity data were acquired every 10 s using a Lockheed Martin BGM-5 dynamic gravimeter during the cruise. The data were corrected for the drift of the instrument during the cruise using land attachments and manually cleaned from outliers. The gravity anomaly along the profile Sanba 3 is smooth along the entire basin and shows clear peaks correlated to basement highs on the Sao-Paulo Plateau. Because seismic velocities and densities are often correlated, gravity modelling provides important additional information on the seismic model. Areas unconstrained by the seismic data can be further constrained by gravity modelling. In a first step, the average velocities of each layer from the seismic model were converted to densities using the empirical relationship from Ludwig *et al.* (1970). The upper-mantle densities were set to a constant 3.32 g cm^{-3}, consistent with the upper-mantle velocities of 8.00–8.20 km s^{-1} found from the seismic data. The gravity anomaly from shipboard measurements along the profile was used for gravity modelling (Fig. 13). To avoid edge effects, the model was extended 200 km at both ends and down to a depth of 95 km. The resulting predicted gravity anomaly along the profile shows a good fit to the shipboard measured gravity anomaly. The largest misfit of about 10 mGal can be observed at the westernmost end of the model and may be an edge effect.

5 COMPARISON WITH THE REFLECTION SEISMIC DATA

The wide-angle velocity models show good agreement with the reflection seismic section (Fig. 2). The most prominent sedimentary reflectors and the basement reflector were digitized from the reflection seismic section and incorporated into the forward modelling with slight adjustments where necessary to fit the OBS data. Very steep reflectors identifiable for example in the basement topography in the reflection seismic data at the eastern flank of the Sao-Paulo Platform can lead to instability of the ray tracing algorithm. However, only sedimentary reflectors discernible in the OBS data and therefore necessary for the modelling were included to avoid overparametrization of the inversion. Velocities of these main

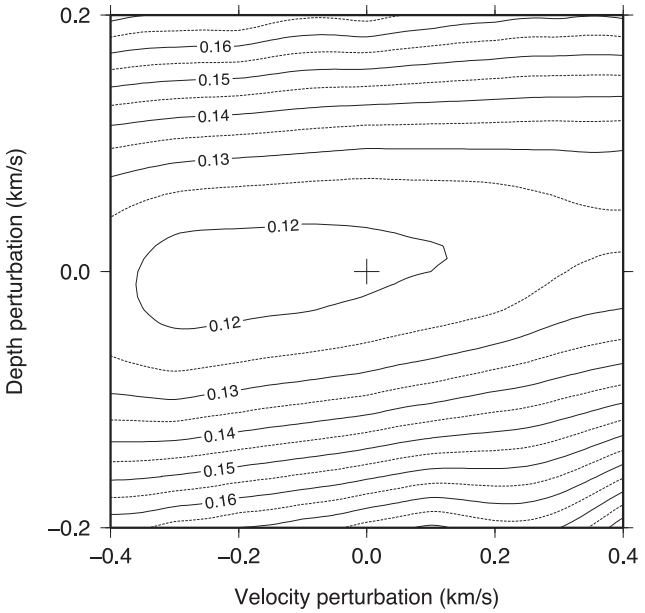

Figure 9. Uncertainty analysis of the forward model by perturbation of the depth of the Moho and velocity of the lower crustal layer. Variation of the resulting RMSE is contoured. All given nodes were varied simultaneously.

sedimentary layers were constrained by wide-angle seismic data, but some additional layering is imaged by the reflection seismic data, especially in the second sedimentary layer along the basin. Depth of the acoustic basement is in very good agreement along the complete model, except in some very steep parts of the record section. Reflections from the Moho are sparse in the MCS section, with some reflected energy around 9.5 s TWTT coinciding with the Moho discontinuity from the forward model.

6 RESULTS AND DISCUSSION

The main objectives of the Sanba cruise along profile Sanba 3 were to constrain the nature of the crust in the easternmost Santos basin and Sao-Paulo Platform. Modelling and interpretation of the wide-angle seismic data from the Sanba 3 profile allowed us to identify three distinct regions (Fig. 14). The first region between 0 and 130 km model distance comprises the southern flank of the Sao Paulo Plateau and the Sao Paulo Ridge with a crustal thickness of up to 17 km. The second region, located between 130 and 300 km model distance is the easternmost Santos Basin comprising up to 4-km-thick sedimentary layers and underlain by a roughly 5-km-thick crust. The easternmost region between 280 and 320 km model distance is characterized by a steep basement high and further east again roughly 5-km-thick crust.

6.1 The Sao-Paulo Plateau Ridge: thinned continental crust

In the first region two sedimentary layers have been modelled using velocities from 2.2–2.3 km s^{-1} and 2.5–3.2 km s^{-1}. The thickness of the sedimentary layers is about 2–3 km. Interbedded into the two layers is a thin layer with velocities between 4.5 and 4.75 km s^{-1}, presenting a velocity inversion with respect to the second sedimentary layer. It was necessary to include this feature into the model, as the velocity inversion can be clearly seen as a typical 'step back' in the record sections of five OBS (Fig. 15). An explanation for this layer might be a volcanic sill or a carbonate layer, which are both characterized by seismic velocities higher than 4 km s^{-1}. The existence of basaltic fragments in the DSDP drillhole 356 might indicate the existence of basaltic flows in the region. Coincidentally, the magnetic data along the profile show a positive anomaly in this region (Fig. 14a). A third explanation might be the presence of salt, however the top of this layer does not show undulations which are characteristic for salt layers and the layer itself shows internal layering, which would not be expected for a salt layer. The crust underneath the sedimentary layers is divided into two layers of roughly similar thickness with velocities ranging from 5.2 to 6.4 km s^{-1} and from 6.6 to 6.9 km s^{-1}, resulting in low velocity gradients. Seismic velocities, relative layer thickness and low velocity gradients are characteristic for thinned continental crust. Comparison of 1-D velocity depth profiles of the crust and upper mantle in this region to those of thinned continental crust from Christensen & Mooney (1995), confirms that the nature of the ridge is thinned continental (Fig. 14c). This has been proposed by others (Chang *et al.* 1992; Blaich *et al.* 2011; Kumar *et al.*

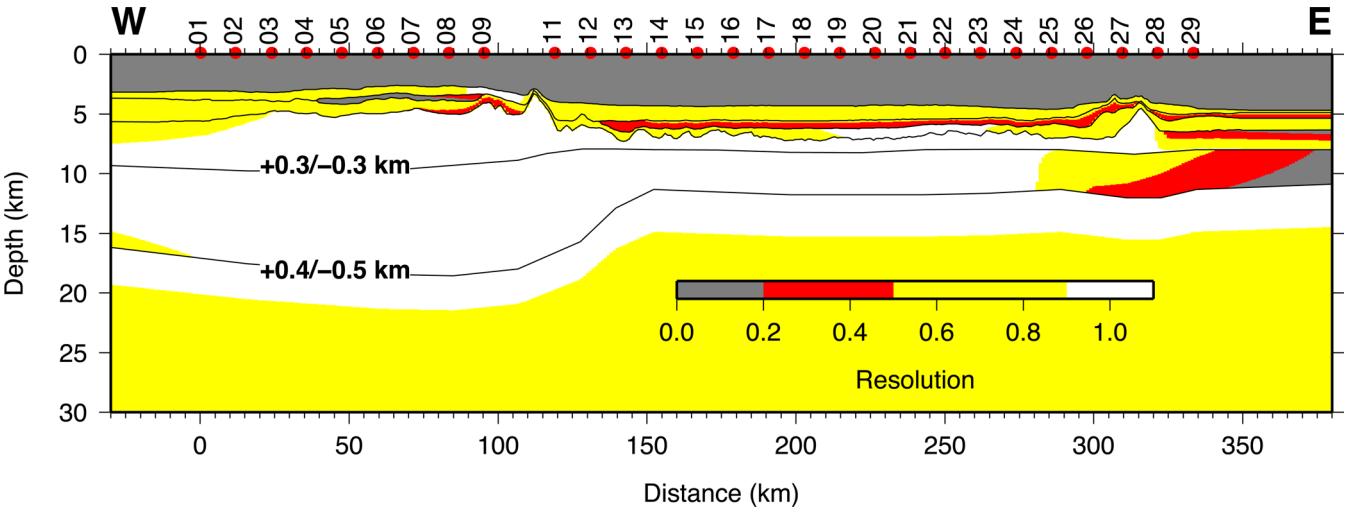

Figure 10. Resolution parameter for all depth nodes of the velocity model of Sanba 3. OBS positions are marked by red circles. Annotations give the depth uncertainty of the most important boundaries calculated from the 95 per cent confidence limit of the *F*-test.

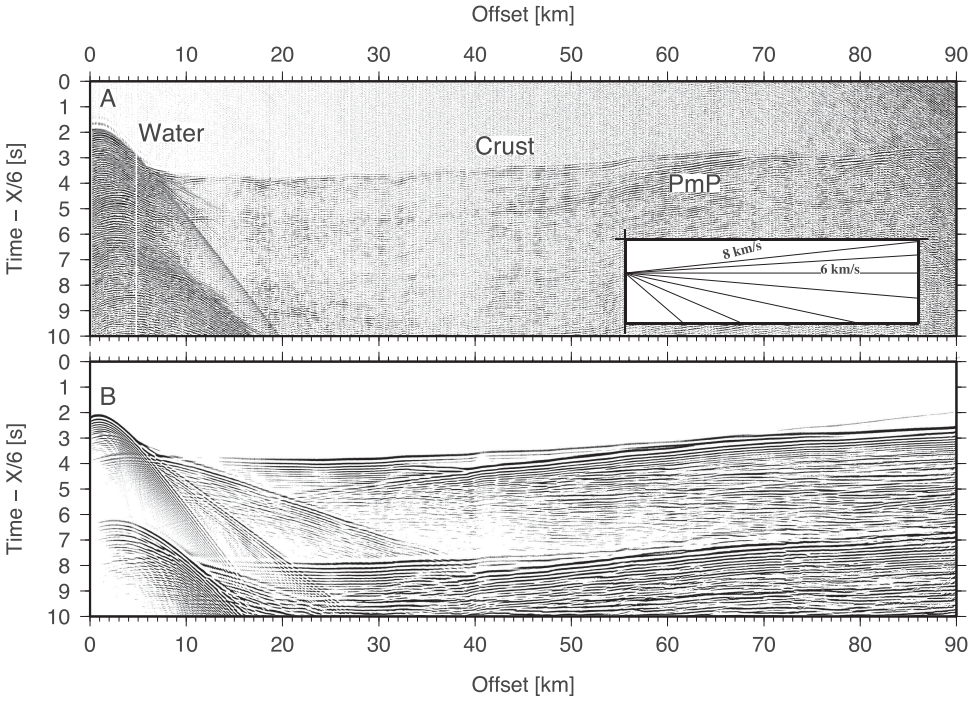

Figure 11. (a) Bandpass filtered (3–5 Hz, 24–36 Hz) vertical geophone data section from OBS 01. The data are displayed with a gain proportional to source-receiver offset and are reduced at a velocity of 8 km s^{-1}. PmP (reflection from the Moho), and Pn (turning waves from the upper mantle) are annotated. (b) Synthetic seismograms calculated from the velocity model for the same station using the finite-difference modelling code from the Seismic Unix package (Stockwell 1999; Cohen & Stockwell 2003). The synthetic seismograms are calculated every 100 m with a source frequency centred around 5 Hz.

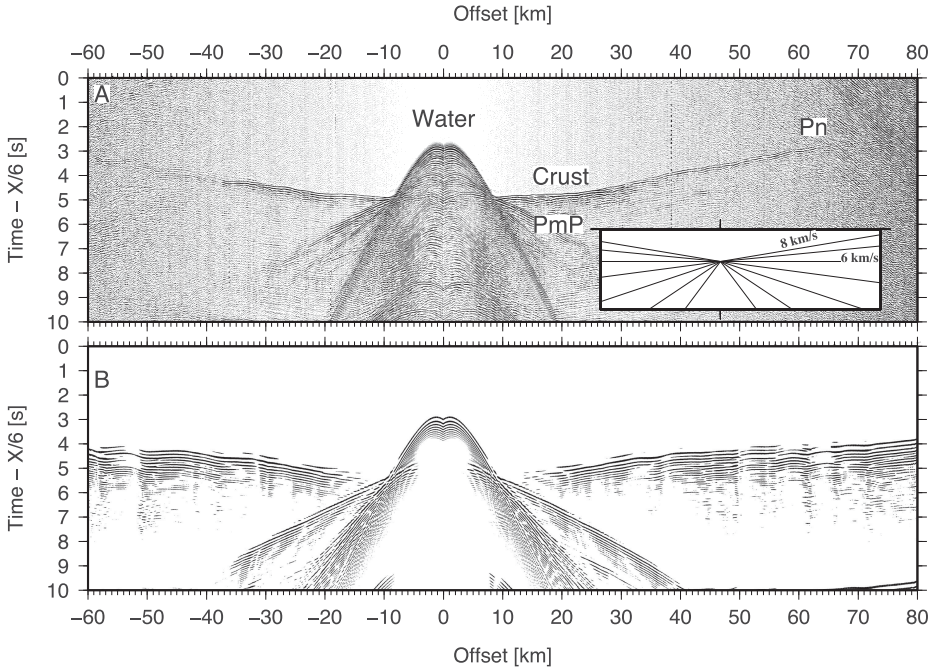

Figure 12. (a) Bandpass filtered (3–5 Hz, 24–36 Hz) vertical geophone data section from OBS 19. The data are displayed with a gain proportional to source-receiver offset and are reduced at a velocity of 8 km s^{-1}. PmP (reflection from the Moho), and Pn (turning waves front he upper mantle) are annotated. (b) Synthetic seismograms calculated from the velocity model for the same station using the finite-difference modelling code from the Seismic Unix package (Stockwell 1999; Cohen & Stockwell 2003). The synthetic seismograms are calculated every 100 m with a source frequency centred around 5 Hz.

2012). This hypothesis is in good agreement with the kinematic evolution, and the presence of a microcontinental block proposed by Moulin *et al.* (2012). The upper mantle is modelled using velocity of 8.0–8.2 km s^{-1}, typical for unaltered mantle peridotites. Thus no indications for mafic underplate, related to the small scale volcanic activity proposed earlier, or serpentinization of the upper mantle as proposed by Zalan *et al.* (2011) are found in this region of thinned continental crust.

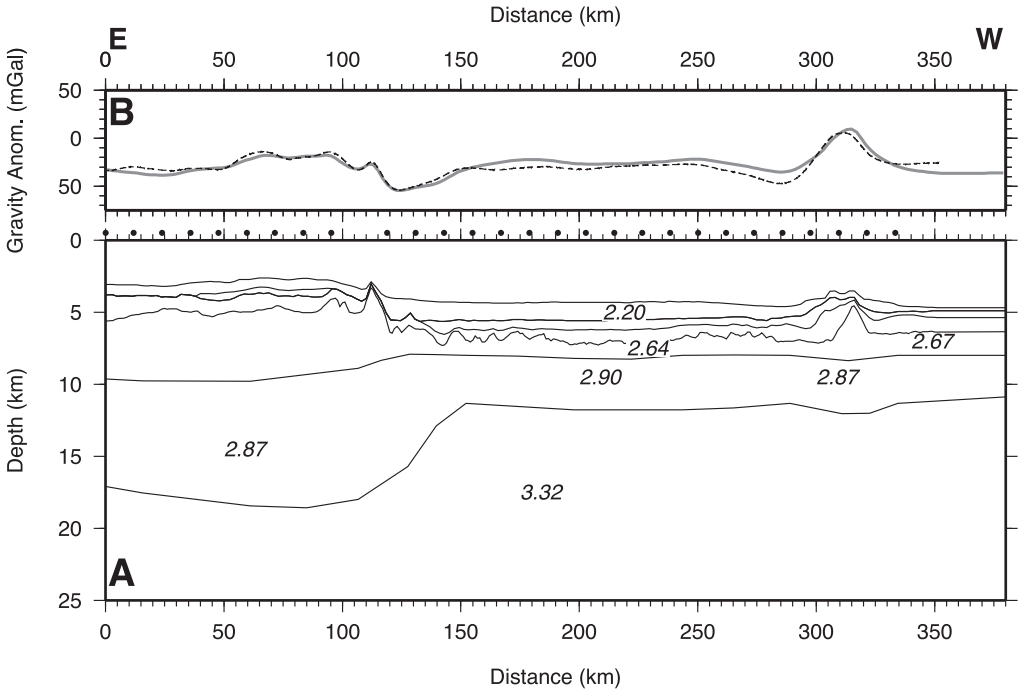

Figure 13. Results of the gravity modelling of profile Sanba 3. (a) Density model boundaries. Densities used during the modelling are annotated. (b) Shipboard measured gravity anomaly (solid line) and calculated anomaly from the modelling (dashed line). A linear trend has been subtracted from the data, since this long-wavelength signal may have its origin in the deeper mantle.

6.2 The easternmost Santos Basin: serpentinized upper mantle or thin oceanic crust?

The second domain imaged on profile Sanba 3, between 150 and 290 km model distance, corresponds to the easternmost SantosBasin. This basin forms a triangle at the southeast end of the SSPS, bounded by the Cruzeiro do Sul Lineament and Jean Charcot Seamounts, the FFZ and the neighbouring continental domain. Sedimentary layers in this domain are substantially thicker than in the SSPS, with a combined thickness of up to 4 km. Three distinct sedimentary layers where modelled in this region, including velocities between 2.1–2.2, 2.4–2.5 and 3.4–3.6 km s^{-1}. The seismic velocities of the sedimentary layers increase about 0.2 km s^{-1} towards the west. No velocity inversion has been detected in this region. The underlying crust is about 5 km thick and separated into two layers. The upper layer is between 1–1.5 km thick and velocities ranging from 6.2 to 7.0 were used to model it. The lower layer is around 4.5 km thick and characterized by velocities ranging from 6.7 to 7.0 km s^{-1}. Three hypotheses can be made for the nature of the crust in this region: continental crust possibly overlying serpentinized mantle, exhumed mantle or atypical thin oceanic crust.

6.2.1 Very thin continental crust

Based on wide-angle seismic profiles, very thin continental crust was proposed to exist on several passive continental margins, for example Nova Scotia (Funk *et al.* 2004), and Morocco (Contrucci *et al.* 2004; Fig. 16a). The crust in these regions is mostly characterized by two layers with low velocity gradients. Based on *P*- and *S*-wave modelling of wide-angle seismic data, thin upper and middle continental crust underlain by serpentized mantle has been proposed to exist at the Flemish Cap margin (Gerlings *et al.* 2012).

A different type of thinned continental crust with velocities similar to those imaged along the Sanba 3 profile was proposed to exist at the Iberian margin south of the Tagus Abyssal Plain. Here, the ocean–continent transition (OCT) zone is marked by two distinct layers with velocities from roughly 6.0–6.3 km and 6.4–7.2 km s^{-1} and modelling of the data from this region required two velocity steps, one at the intracrustal layer boundary and one at the Moho. Both correspond to changes in the reflectivity observed on the MCS data (Afilhado *et al.* 2008; Fig. 16b). Based on these findings the authors propose an upper crustal layer composed of thinned continental crust overlying a heterogeneous layer of gabbros or serpentinized peridotites. Although the velocity–depth profiles match very well with those from Sanba 3, the relative layer thickness distribution differs significantly. In the Iberian margin both layers have a thickness of around 2–3 km, and in the Sanba basin the upper layer is significantly thinner, around 1–1.5 km (Fig. 16d). The thin continental layer is about 4 km thick, similar to crust found in the Santos basin along the profile Sanba 3. However the relative layer thickness in this domain, does not correspond to values found for thinned continental crust (Fig. 16a).

Extreme thinning of continental crust will be accompanied by embrittlement of the crust, as it thins and cools. Although part of the thinning might occur along small faults, not identifiable in the seismic section or by polyphase faulting when several generations of faults cut through the crust obscuring earlier fault-systems (Reston & McDermott 2014), it seems unrealistic to propose that continental crust can thin uniformly to this thickness without fracturing at least partially into identifiable blocks. This leads us to propose, based on the seismic velocities and the deep crustal structure, that the crust in the basin of profile Sanba 3 is not constituted of continental crustal material.

6.2.2 Exhumed mantle

A second explanation of the origin of the crust in the basin might be, that it represents continental mantle, exhumed during the last phase

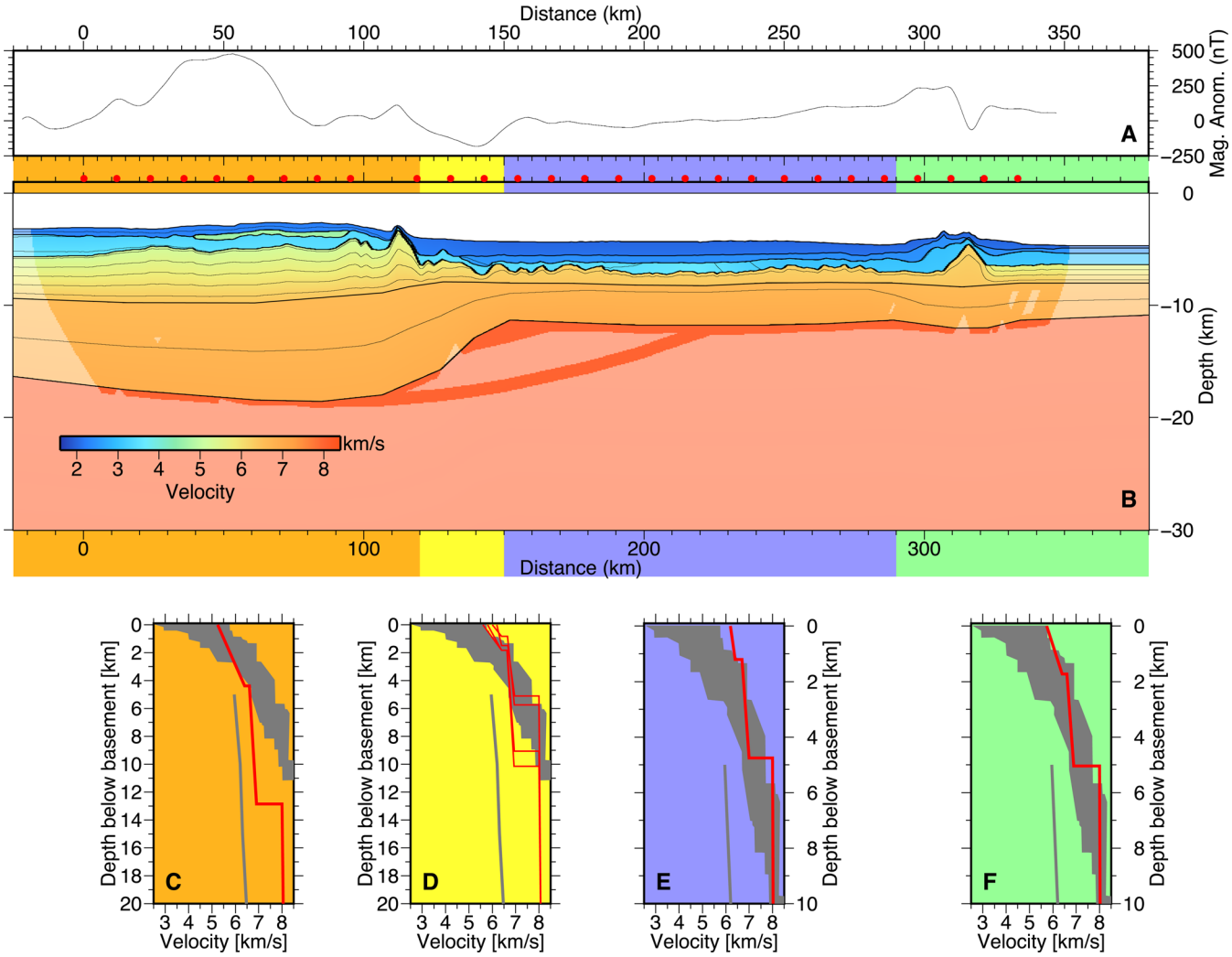

Figure 14. (a) Shipboard measured magnetic anomaly along the profile Sanba 3. (b) Final velocity model of Profile Sanba 3. Velocities are contoured at an 0.25 km s^{-1} interval and black lines mark layer boundaries from the modelling. Red circles mark OBS positions. Orange shading marks extent of the Sao-Paulo Ridge, yellow transition zone between the ridge and the basin, blue the basin and green fracture zone and oceanic crust. (c) Mean of velocity depth curve for profiles taken every 10 km along the green shaded region of the Sao-Paulo Ridge. Grey shaded area marks velocities of typical oceanic crust (White *et al.* 1992) and grey line velocities typical for thinned continental crust (Christensen & Mooney 1995). (d) Velocity depth profiles at 120, 130 and 140 km model distance for the yellow shaded transition zone. (e) Mean of velocity depth curve for profiles taken every 10 km along blue shaded region of the basin. (f) Mean of velocity depth curve for profiles taken every 10 km along green shaded region of the fracture zone.

of continental rifting without volcanic activity which has undergone subsequent serpentinization of the mantle peridotites (Zalan *et al.* 2011). Serpentinized upper mantle material has been drilled at Legs 173 and 149 of the Ocean Drilling Program at the OCT beneath the Iberia Abyssal Plain (ODP Leg 173 scientific party 1998), and its existence has been proposed based on wide-angle seismic data on several passive non-or moderate volcanic margins (e.g. Chian *et al.* 1999; Dean *et al.* 2000; Funk *et al.* 2004; Van Avendonk *et al.* 2006; Afilhado *et al.* 2008; Figs. 16c and d). These margins are interpreted to have formed at the beginning of opening of the basin, when asthenospheric mantle upwelling was too slow to form significant volumes of melt beneath the thinning lithosphere. Although these zones can show a wide span of seismic velocities, they seem to be characterized by high velocity gradients at the top of the basement and a near absence of seismic reflections of reflections from the base of the crust. In the southern Iberian Abyssal Plain a 160-km-wide zone inferred to be exhumed upper mantle has a thickness of 5 km divided into two layers (Dean *et al.* 2000). An upper, high-velocity gradient layer 2–4 km thick, interpreted to be upper mantle peridotite serpentinized along faults between 25 and 100 per cent, which may have subsequently locally been intruded by the products of decompression melting in the mantle and a lower layer up to 4 km thick with a velocity of 7.3–7.9 km s^{-1}, representing mantle peridotite with a mean bulk serpentinization of <25 per cent, possibly concentrated along fewer, but steep-dipping faults. On this profile reflections from the Moho, here representing the serpentinization front, are weak in the wide-angle seismic data and absent in the normal incident data. It is worth noting that this interpretation differs from the one (oceanic crust) proposed by Afilhado *et al.* (2008) for a profile less than 100 km away. Comparison to crust in the basin shows a similar crustal thickness but higher velocities in the upper layer and slightly lower velocities in the lower layer (Fig. 16b).

A 25-km-wide zone of exhumed and serpentinized continental mantle material was proposed to exist along the eastern Grand

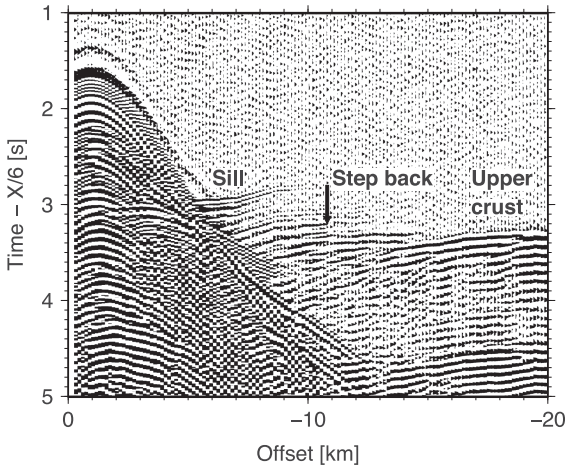

Figure 15. Bandpass filtered (3–5 Hz, 24–36 Hz) data from OBS 05, vertical channel. The data are displayed with gain proportional to source-receiver offset and are reduced at a velocity of 6 km s^{-1}, showing the 'step back' in first arrival times, typical for an inversion of seismic velocities.

Banks margin (Canada), where velocities increase gradually from 6.30 km s^{-1} at the basement to 7.7 km s^{-1} at a depth of 5 km below the basement along a wide-angle seismic profile (SCREECH 2; Van Avendonk *et al.* 2006). This zone coincides with the onset of rough basement topography in the reflection seismic data section. A similar but wider zone was imaged (80 km) on SCREECH line 3 (Lau *et al.* 2006).

Comparison of 1-D velocity–depth (vz) profiles from the Sanba 3 profile with those from the IAM-9 and SCREECH profiles show that crustal thickness is slightly thinner on those profiles and the velocity gradient substantially higher (Figs 16c and d). Also reflections from the Moho can be detected along the Sanba 3 profile (Fig. 2 inset). Therefore, we rule out an origin of exhumed upper mantle for the crust along the Sanba 3 profile.

6.2.3 *Typical, ultraslow or embryonic oceanic crust*

The roughness of oceanic crust increases with decreasing spreading rate, with roughness being inversely proportional to the square root of the spreading rate (Malinverno 1991; Malinverno & Cowie 1993). Studies on very slow spreading ridges in the northern Arctic Ocean show that this simple power law cannot explain the relatively high values from this region (Ehlers & Jokat 2009; Hermann & Jokat 2013). The authors propose a step function fit with a sharp increase of roughness values for slow spreading rates. The basement imaged along the basin on Sanba 3 profile is characterized by a high roughness (Fig. 2). The basin basement imaged along Sanba 3 profile shows a relatively high roughness which might indicate that it originates from very slow spreading.

A comparison to velocity ranges for typical oceanic crust (Fig. 16e) shows that the crust in region is about 2 km thinner than typical oceanic crust and has upper layer velocity higher than those in layer 2 of typical oceanic crust, which corresponds to pillow lavas with typical velocities around 3.5–4 km s^{-1}. The fact that the crust is about 2 km thinner than normal oceanic crust can be explained by accretion at a very slow spreading centre with insufficient melt supply due to low mantle temperatures (Bown & White 1994). Reduced mantle upwelling and conductive heat loss at ultra-slow spreading mid-ocean ridges (less than about 10 mm yr^{-1} half rate) can explain the much thinner (~4 km) crust than normal oceanic crust (6–7 km; White *et al.* 2001). Gabbros appear to make up most of the lower oceanic crust at spreading rates higher than 10 mm yr^{-1} half rate, but at lower spreading rates these intrusives may be retained deeper in the mantle lithosphere (Lizarralde *et al.* 2004). The very thin oceanic crust formed at ultraslow spreading centres might therefore consist of a thin volcanic layer on top of serpentinized mantle rocks (Minshull *et al.* 1998; Jokat & Schmidt-Aursch 2007; Jokat *et al.* 2012). At the Flemish Cap margin, on profile SCREECH 1, Funck *et al.* (2003) argue that the 55-km-wide ocean–continent boundary present a velocity structure compatible with thin oceanic crust created by ultraslow seafloor spreading with limited and/or episodic magma supply operating in parallel with tectonic extension which provided pathways for seawater to reach and partially serpentinize the underlying uppermost mantle. At a very low spreading rate (<20 mm yr^{-1}) this can lead to basaltic lava flows emplaced directly onto serpentinized upper mantle material as proposed for the Southwest Indian Ridge (Muller *et al.* 1997). At slightly higher spreading rates the accreted oceanic crust can consist of basaltic and gabbroic layers but reduced in thickness, for example at Mohns Ridge (Fig. 16g) where layer 2 is of variable but mostly normal thickness (2 km) and layer 3 is reduced to 2–3 km (Klingelhofer *et al.* 2000b) or at Knipovich Ridge (Jokat & Schmidt-Aursch 2007). However upper-crustal velocities along the Sanba 3 profile are higher than those found on the Southwest Indian Ridge or Mohns Ridge.

In some marginal basins like the Liguro-Provençal basin, oceanic crust was produced during only short periods at now extinct spreading centres. In this basin, the oceanic crust which is clearly defined by seismic data show no coherent magnetic anomalies (Gailler *et al.* 2009; Aslanian & Moulin 2012, Moulin *et al.* in press; Fig. 16h), therefore the acretion process must have differed from fully developed mid-ocean ridges. The comparison between vz-profiles of the Sanba 3 profile and vz-profiles obtained on the crust of oceanic origin in the Liguro-Provençal basin exhibits strong similarities in thickness and velocity gradients between these two domains and both curves fit well, suggesting the accretion process may have been similar in both cases. An extinct spreading centre might be present at a rifted margin, if a ridge jump happened soon after continental breakup.

Recent studies of drill samples show, that the first proto-oceanic crust created at onset of spreading – can incorporate high amounts of serpentinite underlying a layer of MORB-type basalt (Jagoutz *et al.* 2007; Tucholke *et al.* 2007), analogue to oceanic crust created at ultra-slow spreading rates. At first the amount of basalt is highly variable at a small wavelength which the wide-angle seismic method is not able to resolve.

A second argument that the crust imaged in the basin is different from typical oceanic crust or thin but igneous oceanic crust, is the amplitude and the shape of the Moho reflection. Along Sanba profile SB-1, which crosses Sanba 3 at 180 km model distance, in the purely oceanic region south-west of the FFZ, the Moho is imaged continuously as a high amplitude reflector (Figs 1 and 17). Northwest of the fracture zone the deep reflector is imaged although with a much weaker amplitude and less continuously (Fig. 17), which might confirm the presence of relatively high amounts of intrusion of peridotites in the lower crust.

6.2.4 *Seamount and thin oceanic crust*

Profile Sanba 3 crosses a seamount at 320 km model distance and extends about 30 km onto oceanic crust (Fig. 3). This region is

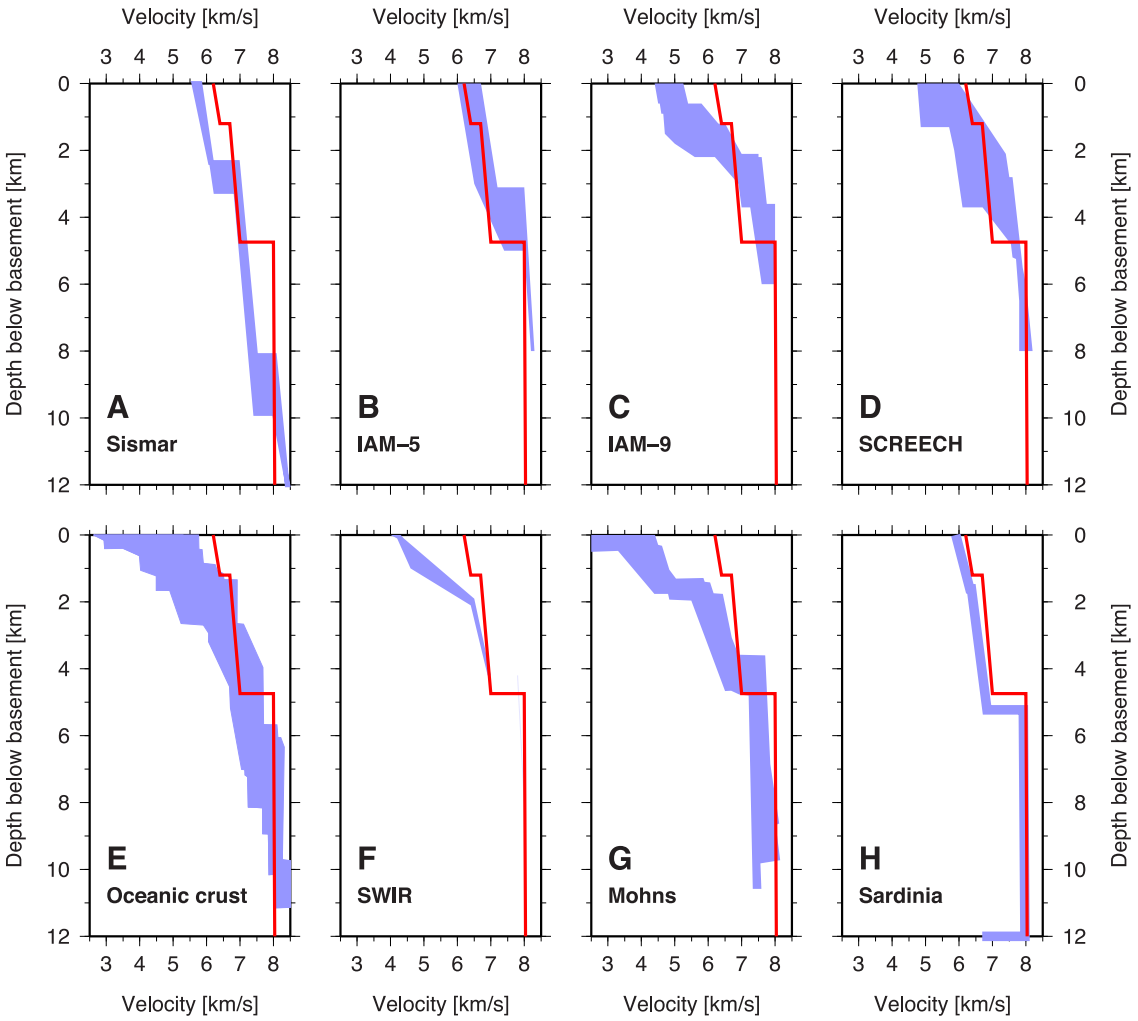

Figure 16. Comparison of the mean vz-profile from the basin with other seismic refraction studies. (a) Vz-profile of Sanba 3 and blue shaded area which marks velocities from thinned continental crust offshore Morocco (Contrucci *et al.* 2004). (b) Vz-profiles and blue shaded area which marks velocities of serpentinized upper mantle from the IAM-5 profiles at the West Iberia Passive Continental Margin (Afilhado *et al.* 2008). (c) Vz-profiles of, here the blue shaded area marks velocities of serpentinized upper mantle from the IAM-9 profile at the southern Iberia Abyssal Plain (Dean *et al.* 2000). (d) Vz-profiles and blue shaded area which marks velocities of serpentinized upper mantle from the SCREECH profiles at the Grand Banks of Newfoundland (Van Avendonk *et al.* 2006). (e) Vz-profile of Sanba 3 and blue shaded area which marks velocities of typical oceanic crust (White *et al.* 1992). (f) Vz-profile of Sanba 3 and blue shaded area which marks velocities of oceanic crust accreted at the ultraslow spreading Southwest Indian Ridge (Muller *et al.* 2000). (g) Vz-profile of Sanba 3 and blue shaded area which marks velocities of oceanic crust accreted at the very slow spreading Mohns Ridge (Klingelhofer *et al.* 2000a). (h) Vz-profiles and blue shaded area which marks velocities of thin back-arc basin crust in the Liguro-Provencal Basin (Klingelhoefer *et al.* 2007).

less well constrained than the Sao Paulo Plateau or easternmost Santos Basin (Fig. 16) and comparison of the vz profiles from this region show that velocities and velocity gradients are in good agreement with oceanic crust. However, the thickness of around 5 km is less than that for typical oceanic crust (White *et al.* 1992; Fig. 3), which might be explained by slow or very slow spreading rates during accretion. Moho reflections in the MCS data are of higher amplitude than those from the basin (Fig. 17). Based on the velocity depth distribution, the reduced crustal thickness and the well-imaged Moho reflections, we propose that the crust in this region is thin oceanic crust, probably formed at slow or very slow spreading rates, as observed for example at the very slow spreading southwest Indian Ridge (Muller *et al.* 1997) and at Mohn's Ridge (Klingelhofer *et al.* 2000b). The lower crust may include a small amount of upper mantle material.

7 CONCLUSIONS

Tomographic and forward modelling of wide-angle seismic data from a 380-km-long profile off the Brazilian coast shows:

(1) The Sao Paulo Ridge is underlain by a 16-km-thick crust of continental affinity. A high velocity layer is imaged in the sedimentary layers overlying the ridge, and might correspond to basaltic lava flows, as they are correlated to a positive magnetic anomaly.

(2) The crust in the easternmost part of the Santos basin is characterized by two layers. The upper layer is between 1 and 1.5 km thick and velocities ranging from 6.2 to 7.0 were used to model it. The lower layer is around 4.5 km thick and characterized by velocities ranging from 6.7 to 7.0 km s^{-1}. It's thickness is about 2 km thinner and velocities are higher than typical oceanic crust. We

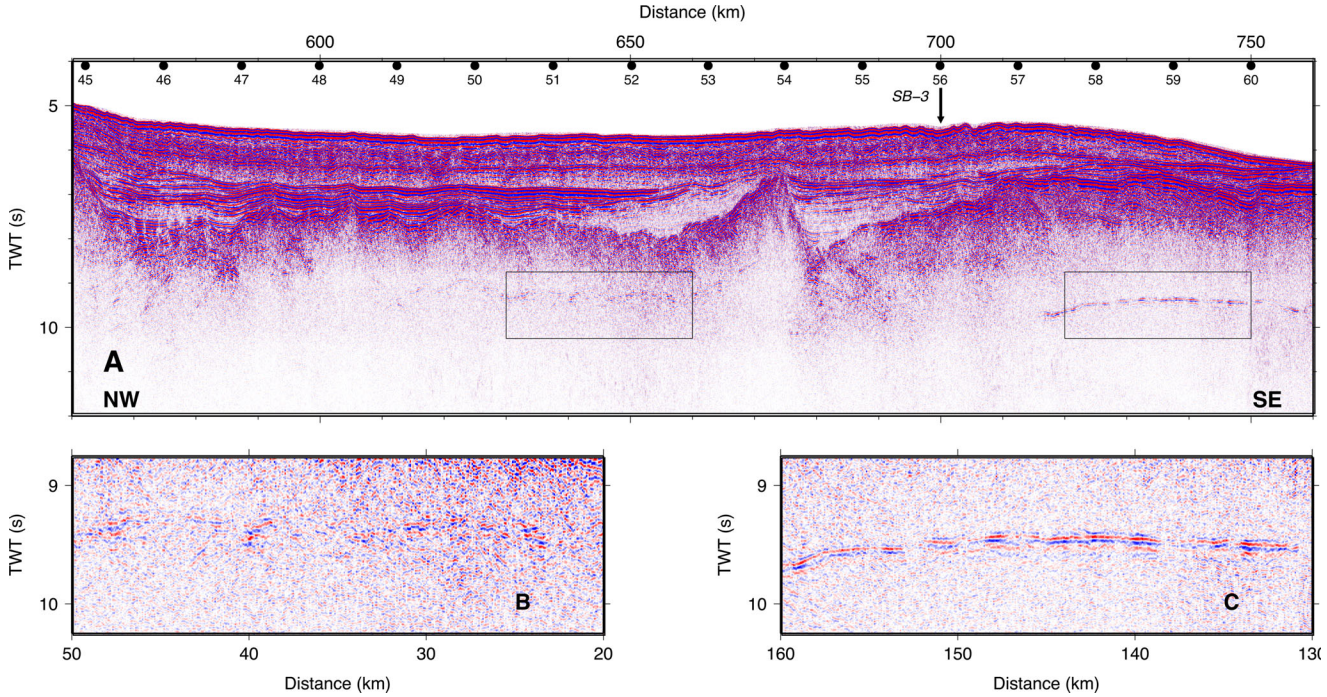

Figure 17. Reflection seismic section of profile SB-1. Comparison of the deep reflection in the oceanic domain and in the basin northwest of the Florianopolis fracture zone. (a) MCS section with location of the two reflectors. (b) Blow-up of the deep reflector in the northwestern part. (b) MCS section of the deep reflector in the southeastern part.

propose this crust to be proto-oceanic crust, accreted at the onset of seafloor spreading, at subdued spreading rates.

(3) East of a fracture zone imaged on our profile, more mature oceanic crust is imaged and interpreted to have formed during from slow or very slow spreading.

ACKNOWLEDGEMENTS

We would like to thank the captain and the crew of the R/V L'Atalante as well as the OBS, landstations and MCS technical teams who made this experiment possible. The GMT (Wessel & Smith 1998) and Seismic Unix software package (Stockwell 1999) were used in the preparation of this paper. We would like to thank H. van Avendonk, W. Jokat and one anonymous reviewer for constructive and detailed reviews which substantially improved the quality of the manuscript. We thank M.-A. Gutscher for help with the English.

CONTRIBUTIONS

The SANBA Project was led by D. Aslanian and M. Moulin, from Ifremer, and A. Viana, from Petrobras. Modelling of the Sanba 3 profile was done by F. Klingelhoefer and modelling of the neighbouring wide-angle seismic profiles of the project by M. Evain, A. Afilhado, C. Rigoti, A. Loureiro D. Alves, A. Leprêtre and A. Feld. Processing of the deep sounding reflection seismic data was done by P. Schnurle and that of the high resolution seismic data by M. Benabdellouahed, A. Baltzer and M. Rabineau.

REFERENCES

Afilhado, A., Matias, L., Shiobara, H., Hirn, A., Mendes-Victor, L. & Shimamura, H., 2008. From unthinned continent to ocean: the deep structure of the West Iberia passive continental margin at 38°N, *Tectonophysics*, **458**, 9–50.

Alvey, A., Kusznir, N.J. & Roberts, A.M., 2011. Detached micro-continents offshore southern Brazil: Crustal thickness from gravity inversion and plate reconstructions, in *Proceedings of the AAPG Annual Conference and Exhibition*, 10–13 April 2011, Houston, TX. AAPG, Search and Discovery Article, 90124.

Aslanian, D. & Moulin, M., 2012. Palaeogeographic consequences of conservational models in the South Atlantic Ocean, *Geol. Soc., Lond., Spec. Publ.*, **369**(1), 75–90.

Aslanian, D. *et al.*, 2009. Brasilian and Angolan passive margins: the kinematic constraints, *Tectonophysics, Spec. Issue: Role of the Magmatism*, **468**, 98–112.

Austin, J.A. & Uchupi, E., 1982. Continental–oceanic crustal transition off Southwest Africa, *Am. Assoc. Petrol. Geol. Bull.*, **66**, 1328–1347.

Blaich, O.A., Faleide, J.I. & Tsikalas, F., 2011. Crustal breakup and continent-ocean transition at South Atlantic conjugate margins, *J. geophys. Res.* **116**, B01402, doi:10.1029/2010JB007686.

Bown, J.W. & White, R.S., 1994. Variation with spreading rate of oceanic crustal thickness and geochemistry, *Earth planet. Sci. Lett.*, **19**, 25–36.

Chang, H.K., Kowsmann, R.O., Figueiredo, A.M.F. & Bender, A.A., 1992. Tectonics and stratigraphy of the East Brazil Rift System: an overview, in ed. Ziegler, P.A., Geodynamics of Rifting; Volume II, Case History Studies on Rifts; North and South America and Africa, *Tectonophysics*, **213**, 97–138.

Chian, D., Louden, K.E., Minshull, T.A. & Whitmarsh, R.B., 1999. Deep structure of the ocean-continent transition in the southern Iberia Abyssal Plain from seismic refraction profiles: Ocean Drilling Program (Legs 149 and 173) transect, *J. geophys. Res.*, **104**, 7443–7462.

Christensen, N.I. & Mooney, W.D., 1995. Seismic velocity structure and composition of the continental-crust—a global view, *J. geophys. Res.: Solid Earth*, **100**(B6), 9761–9788.

Cohen, J.K. & Stockwell, J.W., 2003. Seismic Unix Release 37: a free package for seismic research and processing, Center for Wave Phenomena, Colo. Sch. of Mines, Golden, CO.

Contrucci, I. *et al.*, 2004. The crustal structure of the NW Moroccan continental margin from wide-angle and reflection seismic data, *Geophys. J. Int.*, **159**(1), 117–128.

Curie, D., 1984. Ouverture de l'Atlantique sud et discontinuités intra-plaque: une nouvelle analyse, *PhD thesis*, Université de Bretagne Occidentale, Brest, 192 pp.

Dean, S.M., Minshull, T.A., Whitmarsh, R.B. & Louden, K.E., 2000. Deep structure of the ocean-continent transition in the southern Iberia Abyssal Plain from seismic refraction profiles: the IAM-9 transect at 40° 20′N, *J. geophys. Res.*, **105**(B3), 5859–5885.

Ehlers, B.M. & Jokat, W., 2009. Subsidence and crustal roughness of ultra-slow spreading ridges in the northern North Atlantic and the Arctic Ocean, *Geophys. J. Int.*, **177**(2), 451–462.

Funck, T., Hopper, J.R., Larsen, H.C., Louden, K.E., Tucholke, B.E. & Holbrook, W.S., 2003, Crustal structure of the ocean-continent transition at Flemish Cap: seismic refraction results, *J. geophys. Res.*, **108**(B11), doi:10.1029/2003JB002434.

Funk, T., Jackson, H.R., Louden, K.E., Dehler, S.A. & Wu, Y., 2004, Crustal structure of the northern Nova Scotia rifted continental margin (Eastern Canada), *J. geophys. Res.*, **109**(B9), doi:10.1029/2004JB003008.

Gailler, A., Klingelhoefer, F., Olivet, J.L. & Aslanian, D., 2009. Crustal structure of a young margin pair: new results across the Liguro–Provencal Basin from wide-angle seismic tomography, *Earth planet. Sci. Lett.*, **286**(1), 333–345.

Gerlings, J., Louden, K.E., Minshull, T.A. & Nedimović, M.R., 2012. Flemish Cap–Goban Spur conjugate margins: new evidence of asymmetry, *Geology*, **40**(12), 1107–1110.

Gradstein, F.M., Ogg, J.G. & Smith, A.G., 2004. *A Geologic Time Scale*, Cambridge University Press.

Henry, S.G., Kumar, N., Danforth, A., Nuttall, P. & Venkatraman, S. 2010. Mapping the South Atlantic continental-oceanic boundary: rift to early drift along extensional and transform margins, in *Proceedings of the AAPG International Conference and Exhibition, Calgary*, Canada, 12–15 September 2010. AAPG, Search and Discovery Article, 90108.

Hermann, T. & Jokat, W., 2013. Crustal structures of the Boreas Basin and the Knipovich Ridge, North Atlantic, *Geophys. J. Int.*, **193**(3), 1399–1414.

Hinz, K., Neben, S., Schreckenberger, B., Roeser, H.A., Block, M., Souza, K. & Meyer, H. 1999. The Argentine continental margin north of 48 S: sedimentary successions, volcanic activity during breakup, *Mar. Petrol. Geol.*, **16**(1), 1–25.

Jagoutz, O., Müntener, O., Manatschal, G., Rubatto, D., Péron-Pinvidic, G., Turrin, B.D. & Villa, I.M., 2007. The rift-to-drift transition in the North Atlantic: a stuttering start of the MORB machine? *Geology*, **35**(12), 1087–1090.

Jokat, W. & Schmidt-Aursch, M.C., 2007. Geophysical characteristics of the ultraslow spreading Gakkel Ridge, Arctic Ocean, *Geophys. J. Int.*, **168**(3), 983–998.

Jokat, W., Kollofrath, J., Geissler, W.H. & Jensen, L., 2012. Crustal thickness and earthquake distribution south of the Logachev Seamount, Knipovich Ridge, *Geophys. Res. Lett.*, **39**(8), doi:10.1029/2012GL051199.

Klingelhoefer, F., Lafoy, Y., Collot, J., Cosquer, E., Géli, L., Nouzé, H. & Vially, R. 2007. Crustal structure of the basin and ridge system west of New Caledonia (southwest Pacific) from wide-angle and reflection seismic data, *J. geophys. Res.: Solid Earth (19782012)*, **112**, B11102, doi:10.1029/2007JB005093.

Klingelhofer, F., Geli, L., Matias, L., Steinsland, N. & Mohr, J., 2000a, Crustal structure of a super-slow spreading centre: a seismic refraction study of Mohns Ridge, 72° N, *Geophys. J. Int.*, **141**, 509–526.

Klingelhofer, F., Géli, L. & White, R.S., 2000b, Geophysical and geochemical constraints on crustal accretion et the very-slow spreading Mohns Ridge, *Geophys. Res. Lett.*, **27**(10), 1547–1550.

Kumar, N. & Gamboa, L.A.P., 1979. Evolution of the São Paulo Plateau (southeastern Brazilian margin) and implications for the early history of the South Atlantic, *Bull. geol. Soc. Am.*, **90**(3), 281–293.

Kumar, N., Danforth, A., Nuttall, P., Helwig, J., Bird, D.E. & Venkatraman, S. (2012). From oceanic crust to exhumed mantle: a 40 year (1970–2010) perspective on the nature of crust under the Santos Basin, SE Brazil, *Geol. Soc., Lond., Spec. Publ.*, **369**.

Lau, K.W.H., Louden, K.E., Funck, T., Tucholke, B.E., Holbrook, W.S., Hopper, J.R. & Larsen, H.C., 2006. Crustal structure across the Grand-Banks-Newfoundland Basin continental margin—I. Results from a seismic refraction profile, *Geophys. J. Int.*, **167**, 127–156.

Leyden, R., Ludwig, W.J. & Ewing, M., 1971. Structure of continental margin off Punta del Este, Uruguay, and Rio de Janeiro, Brazil, *AAPG Bull.*, **55**(12), 2161–2173.

Lizarralde, D., Gaherty, J.B., Collins, J.A., Hirth, G. & Kim, S.D., 2004, Spreading rate dependence of melt extraction at mid-ocean ridges from mantle seismic refraction data, *Nature*, **432**, 744–747.

Ludwig, J.W., Nafe, J.E. & Drake, C.L., 1970. Seismic refraction, *Sea*, **4**(1), 53–84.

Malinverno, A., 1991. Inverse square-root dependence of mid-ocean-ridge flank roughness on spreading rate.

Malinverno, A. & Cowie, P.A., 1993. Normal faulting and the topographic roughness of mid-ocean ridge flanks, *J. geophys. Res.: Solid Earth (1978–2012)*, **98**(B10), 17 921–17 939.

McKenzie, D., 1978. Some remarks on the development of sedimentary basins, *Earth planet. Sci. Lett.*, **40**(1), 25–32.

Meisling, K.E., Cobbold, P.R. & Mount, V.S., 2001. Segmentation of an obliquely rifted margin, Campos and Santos basins, southeastern Brazil, *AAPG Bull.*, **85**(11), 1903–1924.

Mohriak, W.U., 2001. Salt tectonics, volcanic centers, fracture zones and their relationship with the origin and evolution of the South Atlantic Ocean: geophysical evidence in the Brazilian and West African margins, in, *7th International Congress of the Brazilian Geophysical Society*, Salvador Bahia Brazil, October 2831, 2001, Expanded Abstract, p. 1594.

Moulin, M., Aslanian, D. & Unternehr, P., 2010. A new starting point for the South and Equatorial Atlantic Ocean, *Earth-Sci. Rev.*, **98**(1), 1–37.

Moulin, M., Aslanian, D., Rabineau, M., Patriat, M. & Matias, L., 2012. Kinematic Keys of the Santos-Namibe Basins, in *Geological Society, London, Special Publications*, Vol. 369, eds Mohriak, W.U., Danforth, A., Post, P.J., Brown, D.E., Tari, G.C., Nemcok, M. & Sinha, S.T., Conjugate Divergent Margins. doi:10.1144/SP369.3.

Moulin, F. *et al.*, in press. Deep crustal structure across a young passive margin from wide-angle and reflection seismic data (The SARDINIA Experiment), I. Gulf of Lion's margin, *Bull. Soc. Géol. Français*, special volume ILP.

Muller, M.R., Robinson, C.J., Minshull, T.A., White, R.S. & Bickle, M.J., 1997, Thin crust beneath ocean drilling program borehole 735B at the southwest Indian Ridge?, *Earth planet. Sci. Lett.*, **117**, 295–317.

Muller, M.R., Minshull, T.A. & White, R.S., 2000, Crustal structure at the Southwest Indian Ridge at the Atlantis II fracture zone, *J. geophys. Res.*, **105**, 25 809–25 828.

Minshull, T.A., Muller, M.R., Robinson, C.J., White, R.S. & Bickle, M.J., 1998, Is the oceanic Moho a serpentinisation front ?, in *Modern Ocean Floor Processes and the Geological Record*, Vol. 148, pp. 71–80, eds Mills, R.A. & Harrison, K., Geol. Soc. Spec. Pub.

ODP Leg 173 Shipboard Scientific Party (1998), Drilling reveals transition from continental breakup to early magmatic crust, *EOS, Trans. Am. geophys. Un.*, **79**(14), 173, doi:10.1029/98EO00127.

Perch-Nielsen, K. & Supko, P.R., 1977. Site 356: Sao Paulo Plateau, Deep Sea drilling Project, *Initial Rep.*, **39**, 141–230.

Rabinowitz, P.D. & LaBrecque, J., 1979. The Mesozoic South Atlantic Ocean and evolution of its continental margins, *J. geophys. Res.*, **84**, 5973–6002.

Reston, T. & McDermott, K., 2014. An assessment of the cause of the extension discrepancy with reference to the west Galicia margin, *Basin Res.*, **26**(1), 135–153.

Scotchman, I.C., Gilchrist, G., Kusznir, N.J., Roberts, A.M. & Fletcher, R., 2010. The breakup of the South Atlantic Ocean: formation of failed spreading axes and blocks of thinned continental crust in the Santos Basin, Brazil and its consequences for petroleum system development, in *Petroleum Geology: From Mature Basins to New Frontiers—Proceedings of the 7th Petroleum Geology Conference*, Petroleum Geology Conference Series, 7, pp. 855–866, eds Vining, B.A. & Pickering, S.C. Geological Society, London.

Stica, J.M., Zalan, P.V. & Ferrari, A., 2014. The evolution of rifting on the volcanic margin of the Pelotas Basin and the contextualization of

the Paraná–Etendeka LIP in the separation of Gondwana in the South Atlantic, *Mar. Petrol. Geol.*, **50**, 1–21.

Stockwell, J.W., 1999. The CWP/SU: seismic Unix package, *Comput., Geosci.*, **25**(4), 415–419

Torsvik, T.H., Rousse, S., Labails, C. & Smethurst, M.A., 2009. A new scheme for the opening of the South Atlantic Ocean and the dissection of an Aptian salt basin, *Geophys. J. Int.*, **177**(3), 1315–1333.

Tucholke, B.E., Sawyer, D.S. & Sibuet, J.C., 2007. Breakup of the Newfoundland–Iberia rift, *Geol. Soc., Lond., Spec. Publ.*, **282**(1), 9–46.

Van Avendonk, H., Holbrook, W.S., Nunes, G., Shillington, D., Tucholke, B.E., Louden, K.E., Larsen, H.C. & Hopper, J.R., 2006. Seismic velocity structure of the rifted margin of the eastern Grand Banks of Newfoundland, Canada, *J. geophys. Res.*, **111**, B11404, doi:10.1029/2005JB004156.

Wernicke, B., 1985. Uniform-sense normal simple shear of the continental lithosphere, *Can. J. Earth Sci.*, **22**(1), 108–125.

Wessel, P. & Smith, W.H., 1998. New, improved version of Generic Mapping Tools released, *EOS, Trans. Am. geophys. Un.*, **79**(47), 579–579.

White, R.S., McKenzie, D. & Onions, R.K., 1992. Oceanic crustal thickness from seismic measurements and rare-earth element inversions, *J. geophys. Res.: Solid Earth*, **97**, 19 683–19 715.

White, R.S., Minshull, T.A., Bickle, M.J. & Robinson, C.J., 2001. Melt generation at very slow-spreading oceanic ridges: constraints from geochemical and geophysical data, *J. Petrol.*, **42**(6), 1171–1196.

Zalan, P., Severino, M.C., Rigoti, C.A., Magnavita, L.P., de Oliveira, J.A.B. & Viana, A.R., 2011. An entirely new 3-D-View of the crustal and mantle structure of a south Atlantic passive margin—Santos, Campos and Espirito Santos Basins, Brazil, in *Proceedings of the AAPG Annual Convention and Exhibition*, Extended Abstract, Houston, TX.

Zelt, C. & Barton, P., 1998. Three-dimensional seismic refraction tomography: a comparison of two methods applied to data from the Faeroe Basin, *J. geophys. Res.*, **103**, 7187–7210.

Zelt, C.A., 1999. Modelling strategies and model assessment for wide-angle seismic traveltime data, *Geophys. J. Int.*, **139**(1), 183–204.

Zelt, C.A. & Smith, R.B., 1992. Seismic travel time inversion for 2-D crustal velocity structure, *Geophys. J. Int.*, **108**, 16–31.